inorganics

MDPI

Article

Preparation and DFT Studies of κ^2*C,N*-Hypercoordinated Oxazoline Organotins: Monomer Constructs for Stable Polystannanes

Desiree N. Bender [1], Alan J. Lough [2], R. Stephen Wylie [1], Robert A. Gossage [1] and Daniel A. Foucher [1,*]

[1] Department of Chemistry and Biology, Ryerson University, 350 Victoria Street, Toronto, ON M5B 2K3, Canada; desiree.bender@ryerson.ca (D.N.B.); swylie@ryerson.ca (R.S.W.); gossage@ryerson.ca (R.A.G.)

[2] X-Ray Laboratory, Department of Chemistry, University of Toronto, Toronto, ON M5H 3H6, Canada; alan.lough@utoronto.ca

* Correspondence: daniel.foucher@ryerson.ca

Received: 20 April 2020; Accepted: 11 May 2020; Published: 13 May 2020

Abstract: Tetraorganotin tin(IV) compounds containing a flexible or rigid (**4**: Ph_3Sn-CH_2-C_6H_4-R; **7**: $Ph_3SnC_6H_4$-R, R = 2-oxazolinyl) chelating oxazoline functionality were prepared in good yields by the reaction of lithiated oxazolines and Ph_3SnCl. Reaction of **7** with excess HCl resulted in the isolation of the tin monochlorido compound, **9** ($ClSn[Ph_2]C_6H_4$-R). Conversion of the triphenylstannanes **7** and **4** into their corresponding dibromido species was successfully achieved from the reaction with Br_2 to yield **10** ($Br_2Sn[Ph]C_6H_4$-R) and **11** ($Br_2Sn[Ph]$-CH_2-C_6H_4-R), respectively. X-ray crystallography of **4**, **7**, **9**, **10**, and **11** reveal that all structures adopt a distorted trigonal bipyramidal geometry around Sn in the solid state. Compound **4**, with an additional methylene spacer group, displays a comparatively long Sn–N bond distance compared to the dibromido tin species, **11**. Several DFT methods were compared for accuracy in predicting the solid-state geometries of compounds **4**, **7**, **9**–**11**. Compounds **10** and **11** were further converted into the corresponding dihydrides (**12**: $H_2Sn[Ph]C_6H_4$-R, **13**: $H_2Sn[Ph]$-CH_2-C_6H_4-R), via Br–H exchange, in high yield by reaction with $NaBH_4$. Polymerization of **12** or **13** with a late transition metal catalyst produced a low molecular weight polystannane (**14**: –$[Sn[Ph]C_6H_4$-$R]_n$–, M_w = 10,100 Da) and oligostannane (**15**: –$[Sn[Ph]$-CH_2-C_6H_4-$R]_n$–, M_w = 3200 Da), respectively.

Keywords: hypercoordinate bonding; stannanes; oxazolines

1. Introduction

Polystannanes are main group polymers consisting of chains of covalently bonded tin atoms. These materials possess unique chemical, optical, and electronic properties attributed to the delocalization of the formal Sn 5s electrons into σ–σ bonding orbitals along the backbone [1]. The degree of such delocalization in polystannanes is greater than that noted for comparable Group 14 polymers, (e.g., polysilanes and polygermanes). The Sn analogues display smaller band gaps, greater metallic character, and a visible red shift observed in the UV-Vis spectra [2–4]. A conductivity study by Caseri et al. [5] on undoped poly(di(3-propylphenyl)stannane) found an intrinsic conductivity of 3×10^{-8} Scm^{-1} at 300 K. When Tilley et al. [6] cast films of poly(di-*n*-butylstannane) and poly(di-*n*-octylstannane) doped with SbF_5, conductivities of six to seven orders of magnitude greater (1×10^{-2} and 3×10^{-1} Scm^{-1}) were reported. Unfortunately, both doped and undoped polymers were found to degrade rapidly when exposed to light and/or moisture.

A recent approach to address the sensitivity of polystannanes is to increase the coordination number at the tin center via a pendant functional ligand [7,8]. The benefit of the resulting hypercoordination is

two-fold: first, the addition of a Lewis basic ligand provides additional electron density to the Lewis acidic Sn center and second, the occupation of an additional coordination site hinders nucleophilic attack by creating more congested tin units [9]. The nature of the dative interaction between the additional ligand and the Sn center has been previously rationalized in terms of a three center–four electron (3c–4e$^-$) bond, a concept used to describe hypervalent compounds that exceed the standard octet of valence electrons in Group 14 systems [10–12]. In hypercoordinated Sn (IV) species, 5-coordinate trigonal bipyramidal geometries are preferred and the 3c–4e$^-$ interaction is observed in the assigned axial position (Figure 1). A lone pair of electrons from Y is donated into the non-bonding molecular orbitals of tin and is prominent when X is an electronegative atom such as a halide.

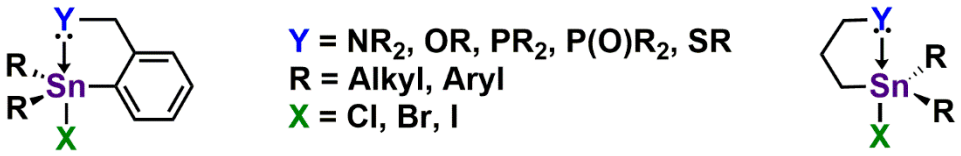

Figure 1. Hypercoordinated triorganotin compounds containing benzyl- (left) and propyl- (right) functionalized ligands.

An early crystallographically characterized example was reported by van Koten et al. [13]. This complex featured an aryl–Sn bond in which the aromatic group contained an ortho-dimethylaminomethyl functionality. A κ^2-*C,N*-bonding motif involving a 5-coordinate Sn atom was observed (Figure 1: R = Ph, Y = NMe_2, X = Br). Several examples of other Group 14 compounds displaying similar hypercoordination have been disclosed since that time [14–16].

Over the last several years, we have reported on the syntheses of asymmetric polystannanes incorporating flexible groups capable of hypercoordination, specifically propyl alkoxy chains containing a hydroxy, phenoxy, biphenyl oxy or oxy azo-benzene moieties [7,8]. These hypercoordinated polystannanes feature a notable increase in stability (>2 months) to both light and moisture compared to their 4-coordinate Sn analogues and display, in most instances, two unique ^{119}Sn NMR resonances. This is presumably due to the presence of both 4- and 5-coordinate tin centers attributed to the flexible side chain containing a donor atom that can move freely to, and away from, tin centers. Polystannanes bearing more rigid groups do not share the same level of flexibility, resulting from a presumed stronger dative interaction and greater steric bulk around the tin units. Recently, we disclosed details on the preparation of hypercoordinate polystannanes with either a benzyl κ^2-*C,N* (dimethylamino) or a κ^2-*C,O* (2-methoxymethyl) chelating group [17]. These materials are derived by dehydropolymerization of the respective –*C,N* and –*C,O* dihydride monomers using a late transition metal catalyst. This leads to the formation of modest molecular weight, amorphous polymers which are stable to both ambient light and moisture.

Another potential class of donor groups that may also be suitable for hypercoordination to Sn are oxazolines (Figure 2: **1a**–**b**). This ring system, also known as 4,5-dihydro-2-oxazoles, are a subclass of azole heterocycles containing an imine nitrogen and an oxygen atom bound by an sp^2 hybridized carbon in a five-membered ring [18]. There have been a limited number of small molecule tin species bearing oxazoline groups reported in the literature [19–25]. Specifically, 2-phenyl-2-oxazolines are particularly interesting as they allow for a potential five-membered chelate ring to be formed when the tin center is bound at the *ortho* position of the aromatic group. The first complex of this nature was also reported by van Koten et al. for [2-(4,4-dimethyl-2-oxazoline)-5-methyl-phenyl]methylphenyltin bromide (Figure 2: **1c**) [26]. X-ray crystallography reveals the nitrogen preferentially datively bonding to the tin center over that of the oxygen atom forming a distorted trigonal bipyramidal geometry around Sn with a relatively short Sn–N bond length (2.414 Å) [23]. The Staliński group later published a series of papers detailing organotin complexes bearing similar chiral oxazoline groups (Figure 2: **2a**–**g**, **3a**–**e**) [27–30]. Evidence of intramolecular Sn–N interactions were probed effectively by ^{1}H, ^{13}C, ^{15}N and ^{117}Sn NMR spectroscopy. Synthesis of these hypercoordinated compounds was achieved via

bromine-lithium exchange from a 2-(2′-bromophenyl)-2-oxazoline ring (*n*-BuLi) followed by reaction with a tin halide species. This work further evaluated the dative interaction structurally by comparing the series of *ortho*- (**2a**–**e**) substituted tin complexes to *para*- (**3a**–**e**) substituted tin analogues where dative interactions are presumably absent. Comparisons of the ^{117}Sn NMR chemical shifts of the series were thereafter given.

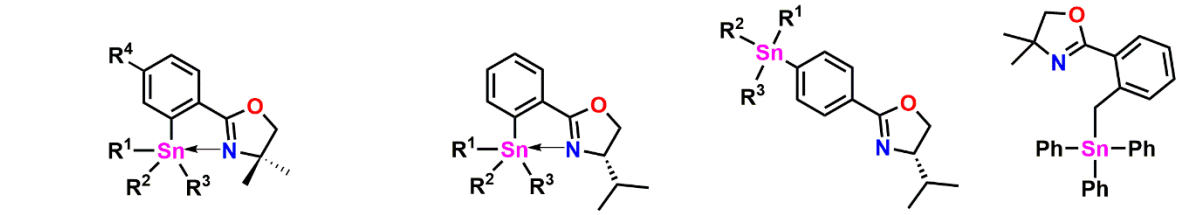

1a: R^1, R^2 = Me, R^3 = Br, R^4 = H
1b: R^1 = Ph, R^2 = Me, R^3 = Br, R^4 = H
1c: R^1 = Ph, R^2 = Me, R^3 = Br, R^4 = Me

2a: R^1, R^2, R^3 = Me
2b: R^1, R^2, R^3 = *n*-Bu
2c: R^1 = Me, R^2 = R^3 = Br
2d: R^1 = *n*-Bu, R^2 = R^3 = Br
2e: R^1 = Me, R^2 = R^3 = H
2f: R^1 = Ph, R^2 = R^3 = Br
2g: R^1, R^2, R^3 = Ph
2h: R^1 = Ph, R^2 = R^3 = H
2i: R^1, R^2 = Me, R^3 = Br
2j: R^1 = *t*-Bu, R^2 = Ph, R^3 = I

3a: R^1, R^2, R^3 = Me
3b: R^1, R^2, R^3 = *n*-Bu
3c: R^1 = Me, R^2 = R^3 = Br
3d: R^1 = *n*-Bu, R^2 = R^3 = Br
3e: R^1 = Me, R^2 = R^3 = H

4

Figure 2. Structures of known tin oxazolines.

This investigation revealed that the ^{117}Sn NMR chemical resonances of complexes **2a**–**e** are shifted significantly upfield relative to the corresponding structural isomers **3a**–**e**. Further evidence of the dative interaction comes from solution ^{15}N NMR spectroscopy of **2a**–**c** where a single nitrogen resonance is detected accompanied by $^{117/119}$Sn satellites. As expected, such tin satellite resonances are absent in **3a**–**3c**. Single crystal X-ray analysis of **2a** reveals a Sn–N bond distance of 2.89(9) Å, while for **2c**, which has a bromido ligand *trans* to the Sn–N bond, possesses a significantly shorter Sn–N bond distance (2.39(2) Å) [27]. These bonds lengths fall well within the sum of the van der Waals radii (~3.72 Å). The shorter bond distance in **2c** is likely a result of the electron withdrawing effects of the bromine on the tin center. One example of a methylene bridged tin oxazoline complex, **4**, (Figure 2) was prepared by Parish and Bonnardel [31]. While no Sn NMR data was reported, the ^{1}H NMR spectrum displays a ^{2}J $^{119/117}$Sn–H coupling constant of 75 Hz for the benzylic protons.

The current work focuses on the suitability of both more rigid and flexible oxazoline tin species as suitable monomers for preparation of light and moisture stable oxazoline containing polystannanes. This rigidity is modified by the incorporation of a methylene spacer group as shown in Figure 3 (cf. **4**).

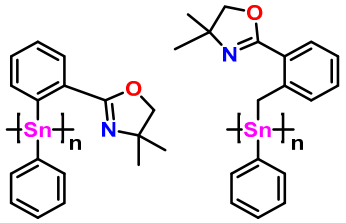

Figure 3. Target tin oxazoline polymers.

2. Results

2.1. Triphenyl Oxazoline Stannanes

Two different synthetic approaches to the tin oxazoline compound **7** (Scheme 1: Route A: 74% yield, Route B: 76% yield) were undertaken. In the first method (Route A), *n*-BuLi was added to an ethereal solution of **5** (cooled to −84 °C) followed by addition of Ph_3SnCl. Trituration with MeOH resulted in the isolation of **7** as a white coloured powder. A second, lower cost method (Route B) adapted from Gschwend et al. [32], where **6** was directly lithiated using *sec*-BuLi, followed by transmetallation with Ph_3SnCl, also yields **7**. ^{119}Sn NMR ($CDCl_3$) spectroscopy of **7** revealed a single resonance (δ = −157.1 ppm), similar to **2g** (Figure 2; ^{117}Sn NMR [$CDCl_3$] δ = −155.5 ppm) [29].

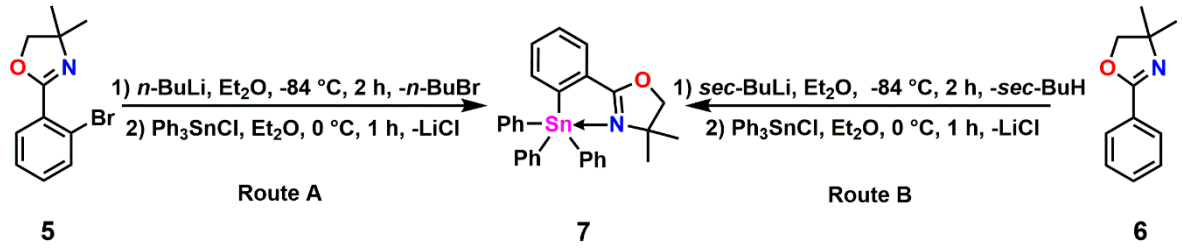

Scheme 1. Synthetic approaches to **7**.

A potentially more flexible oxazoline tin species with a methylene spacer between tin and the aryl group was also pursued. Gschwend et al. [32] had previously demonstrated that the tolyl ring in 4,4-dimethyl-2-(o-tolyl)-4,5-dihydrooxazole (**8**) can be lithiated with *n*-BuLi (Scheme 2) selectively at the methyl group. This lithiated species was shown to be reactive towards various electrophiles; however, no examples with tin were reported. When the ruby red coloured solution of lithiated oxazoline **8** was reacted with Ph_3SnCl, the mixture turned an opaque yellow colour. Following removal of the ethereal solvent, the crude mixture was redissolved in toluene and gravity filtered to remove insoluble materials. After drying in vacuo and trituration of the crude powder with CH_3OH, white coloured crystals of **4** were recovered.

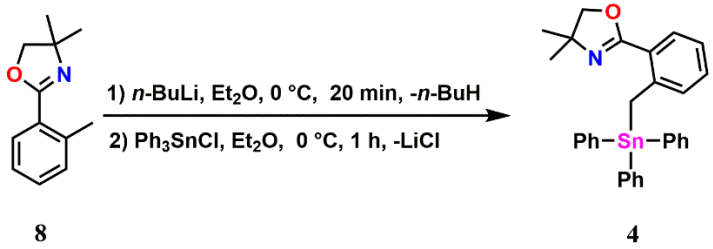

Scheme 2. Synthesis of the semi-flexible methylene-bridged oxazoline stannane **4**.

The ^{1}H NMR ($CDCl_3$) spectrum of **4** reveals a signal corresponding to the benzylic protons located at δ = 3.57 ppm along with $^{117/119}$Sn satellites ($^2J_{1H–117/119Sn}$ = 75.5 Hz) in good agreement with the values reported by Parish [28].

X-ray diffraction studies of both **7** and **4** were undertaken and selected bond lengths and bond angles shown in Table 1. The geometry of the Sn center of **7** is distorted trigonal bipyramidal (τ_5 = 0.92) [33] in nature with the equatorial bond angles around the tin center ranging from 102° to 117° and an axial bond angle of 172.20(6)°. The Sn1–C12 bond of **7** is slightly longer than the other Sn–C aryl bonds in this compound and is likely a result of it being located *trans* to the strongly donating nitrogen atom (Figure 4: top).

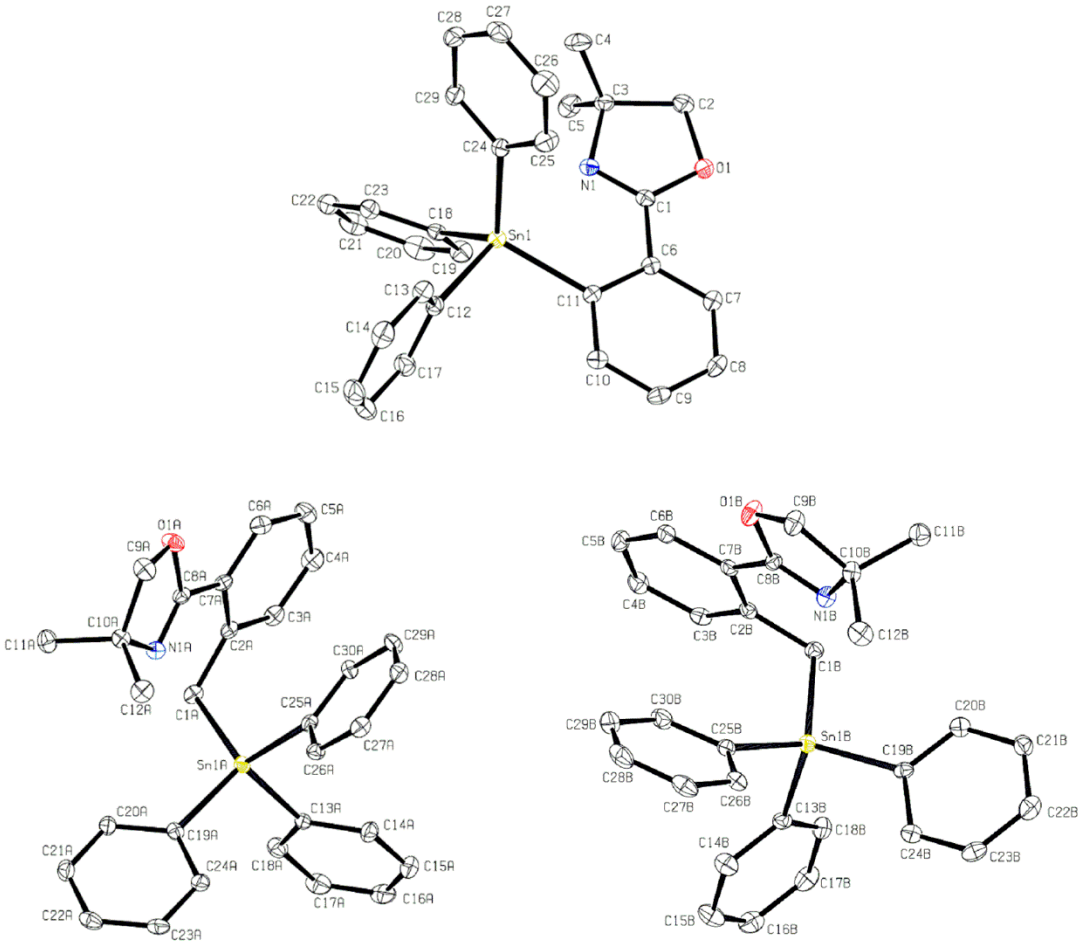

Figure 4. Displacement ellipsoid plots of **7** (top) and the two structurally unique molecules of compound **4** (**4′**: left and **4″**: right bottom) found in the unit cell. Thermal ellipsoids shown at the 30% level.

Table 1. Selected structural data for **7**, **4′**, and **4″**.

Bond Lengths of 7 (Å)		**Bond Lengths of 4′ (Å)**		**Bond Lengths of 4″ (Å)**	
Sn1–N1	2.762(1)	Sn1A–N1A	3.176(4)	Sn1B–N1B	3.234(4)
Sn1–C11	2.1602(16)	Sn1A–C1A	2.162(4)	Sn1B–C1B	2.153(4)
Sn1–C12	2.1752(17)	Sn1A–C13A	2.158(4)	Sn1B–C13B	2.155(4)
Sn1–C18	2.1378(16)	Sn1–C19A	2.150(4)	Sn1B–C19B	2.139(4)
Sn1–C24	2.1425(17)	Sn1–C25A	2.143(4)	Sn1–C25B	2.144(4)
Bond Angles of 7 (°)		**Bond Angles of 4′ (°)**		**Bond Angles of 4″ (°)**	
N1–Sn1–C11	69.83(6)	C1A–Sn1A–C13A	103.61(16)	C1B–Sn1B–C13B	103.30(16)
N1–Sn1–C12	172.20(6)	C1A–Sn1A–C19A	113.46(17)	C1B–Sn1B–C19B	112.07(16)
N1–Sn1–C18	82.20(6)	C1A–Sn1A–C25A	115.46(16)	C1B–Sn1B–C25B	116.09(16)
N1–Sn1–C24	81.81(6)	C13A–Sn1A–C19A	108.28(16)	C13B–Sn1B–C19B	108.41(17)
C11–Sn1–C18	117.09(6)	C13A–Sn1A–C25A	104.86(16)	C13B–Sn1B–C25B	105.81(17)
C12–Sn1–C18	102.03(6)	C19A–Sn1A–C25A	110.34(15)	C19B–Sn1B–C25B	110.34(15)

Hypercoordinated tetraorganotins, such as **7**, possessing a Sn→N interaction are relatively rare. Jurkschat and co-workers reported a Sn–N bond distance of 2.624(8) Å for the sterically confined aza-stannatrane, $MeSn(CH_2CH_2CH_2)_3N$ [34]. The Sn–N bond distance of **7** is 2.762(1) Å and this is

substantially longer than a typical covalent Sn–N bond (~2.15 Å) [35], but well within the sum of their van der Waals radii (3.72 Å). Staliński et al. had reported a Sn–N bond distance of 2.888(9) Å for the closely related compound **2a** (Figure 2) [27].

Two unique molecules of compound **4** (designated as **4′**, **4″**: Figure 4 bottom) were found within the unit cell, both with tin centers adopting a distorted trigonal bipyramidal geometry (τ_5 = 0.80; 0.76, respectively). The equatorial angles around the tin center for both structures are between 103.6° and 116.1° and axial angles of 163.2(1) and 162.0(1)°. The Sn–N (**4′**: 3.176(4) Å, **4″**: 3.234(4)) distances are significantly longer than in **7**, a likely consequence of the additional –CH_2– bridge. A comparison of the solid-state structures of **7**, **4′** and **4″** reveal similar Sn–C bond lengths, with the exception of the Sn–Ph bond *trans* to the oxazoline of **7,** which is elongated compared to the Sn–Ph bond *trans* to the oxazoline ligand of **4′** and **4″**.

2.2. Halogenated Oxazoline Stannanes

Halogenation reactions of both **7** and **4**, leading to dihalido reactive species were investigated. In a method first described by Pannell et al. [36], **7** was treated with one molar equivalent of a 1.0 M solution of HCl/Et_2O for 1 h at RT (Scheme 3).

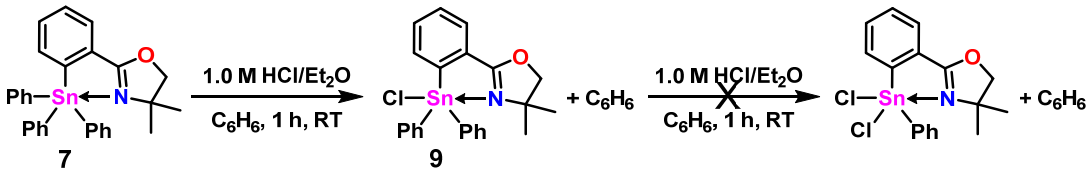

Scheme 3. Attempted sequential chlorination reactions of **7**.

After recrystallization from hexanes, the monochloridostannane **9** was recovered as white coloured powder in an 84% yield. ^{119}Sn NMR ($CDCl_3$) analysis of **9** revealed a single tin resonance (δ = −226.0 ppm), as expected. A successive chlorination attempt to replace a second aryl substituent under the same conditions was unsuccessful (NMR: ^{1}H and ^{119}Sn). Addition of 3- or 4-fold excess of HCl also failed to convert **9** to the desired species. The use of a stronger chlorinating source, $SOCl_2$, was also unsuccessful in conversion to the desired dichlorido species. This methodology was therefore abandoned.

Brominations of **7** and **4** (Scheme 4) were investigated as a possible alternative route to dihalide species. When **7** was reacted with two equivalents of Br_2 (Scheme 4), **10** was obtained in good yield (79%). After solvent removal, a yellow coloured powder remained and ^{119}Sn NMR ($CDCl_3$) analysis revealed a single resonance (δ = −290.6 ppm), which corresponds closely to the shift reported for **2g** (Figure 2, δ_{117Sn} = −288.5 ppm) [30].

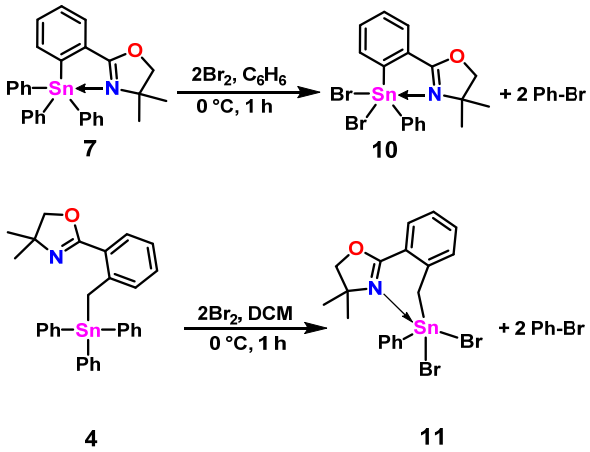

Scheme 4. Bromination of **7** and **4** leading to dibromidos **10** and **11**.

In tin species with potentially hypercoordinating 2-methoxybenzyl or dimethylaminobenzyl groups, replacement of an alkyl or aryl group for an electronegative atom imparts a downfield shift of the ^{119}Sn NMR resonance [9]. However, in the case of **7**, **9**, and **10**, the opposite effect is observed (Figure 5) and upfield ^{119}Sn chemical shifts relative to their four coordinate tin analogs is observed. In the ^{1}H NMR spectra of compounds **7**, **9**, and **10**, the methylene protons of the oxazoline display downfield shifts with each additional halide bound to Sn, possibly a result of inductive effects.

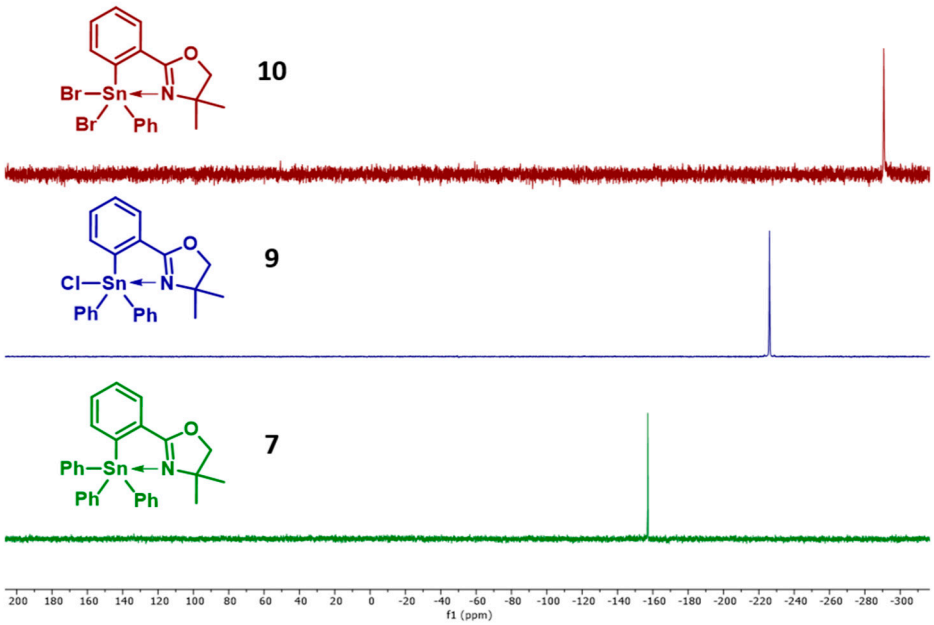

Figure 5. ^{119}Sn NMR spectra ($CDCl_3$) of **7**, **9**, and **10**.

Addition of two equivalents of $Br_2(l)$ to **4** in C_6H_6 was carried out under the same reaction conditions as detailed for **7**. Analysis by NMR revealed the appearance of three tin resonances assigned to the starting material, **4** (the major signal), with two other unassigned resonances at −215 and −248 ppm. When the bromination of **4** was performed in the alternative solvent dry DCM (Scheme 4 bottom), a single ^{119}Sn tin resonance ($CDCl_3$) was detected (δ = −248.2 ppm). After removal of solvent, the crude powder was washed with MeOH, yielding **11** cleanly as a white coloured powder.

Crystals of **9**, **10**, and **11** suitable for single crystal X-ray diffraction analysis were obtained and this investigation revealed (Figure 6) the bond lengths and bond angles shown in Table 2. Two unique molecules of **9** were observed (**9′** and **9″**) within the unit cell of the crystal that differ slightly in terms of bond lengths and angles (*vide infra*).

The geometry around the Sn center in both molecules of **9** is distorted trigonal bipyramidal in nature (**9′**: τ_5 = 0.81, 9″: τ_5 = 0.82) [35]. For both isomers, the angles of N1–Sn–Cl are almost 180°, while the angles between the equatorial atoms range from 117 to 121°. The angles between the axial and the equatorial phenyl groups range between 90 and 95°. The hypothesised 3c–4e$^-$ sharing between the nitrogen, tin and chlorine atoms is supported by an elongated Sn–Cl bond (≈2.49 Å) relative to a typical Sn–Cl bond length (2.41 Å) [33]. The shorter Sn–N bond length found in **9** (2.458 Å) relative to the triphenyltin analogue **7** (2.762 Å) may also be due to an enhanced 3c–4e$^-$ interaction. Staliński et al. reported on the crystal structure of a similar monobromido dimethyltin oxazoline (Figure 2: **2i**) complex that possesses a Sn–N bond distance of 2.39(2) Å [27], significantly shorter than that found in **9**.

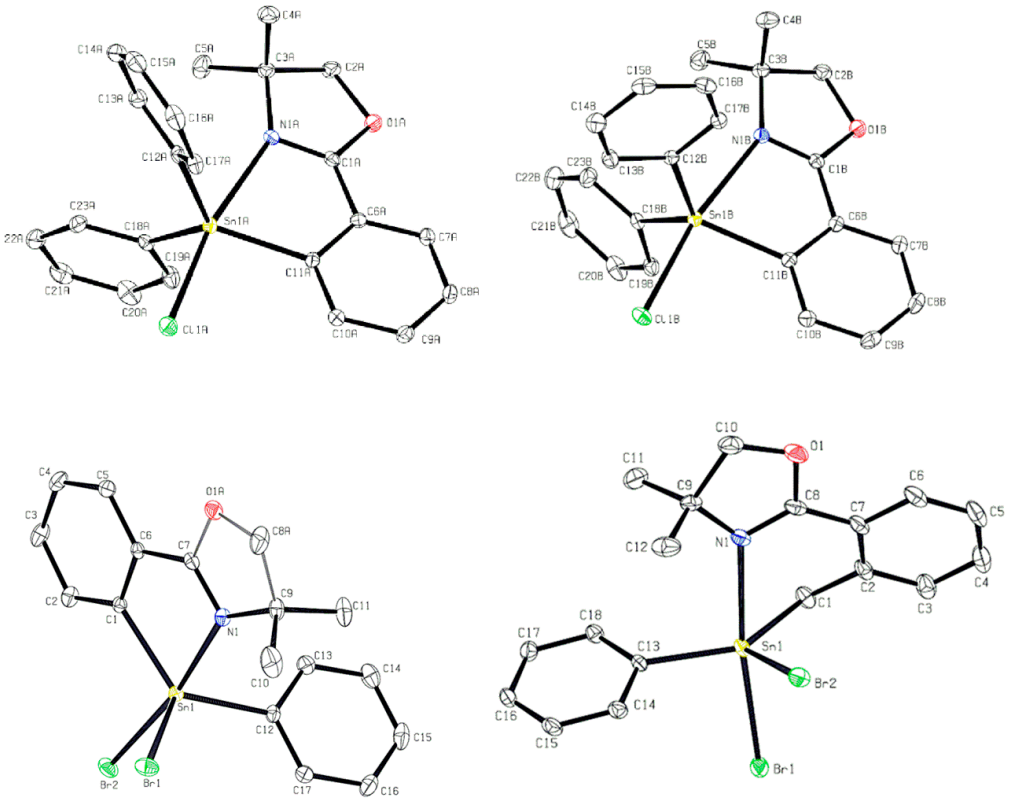

Figure 6. Displacement ellipsoid plots of the two crystallographically independent molecules of compound **9** (top: **9′**: left and **9″**: right) found in the unit cell and compounds **10** (bottom left) and **11** (bottom right). The C7–O1A–C8A–C9–N1 ring of **10** is disordered over two sets of sites. Thermal ellipsoids drawn at the 30% level.

Table 2. Selected structural data for **9**, **10**, and **11**.

Bond Lengths of 9′ (Å)		**Bond Lengths of 9″ (Å)**	
Sn1A–N1A	2.4658(14)	Sn1B–N1B	2.4502(14)
Sn1A–C11A	2.1401(16)	Sn1B–C11B	2.1422(17)
Sn1A–C12A	2.1322(16)	Sn1B–C12B	2.1330(17)
Sn1–C18A	2.1250 (17)	Sn1B–C18B	2.1232(17)
Sn1–Cl1A	2.4832(5)	Sn1–Cl1B	2.4955(5)
Bond Angles of 9′ (°)		**Bond Angles of 9″ (°)**	
N1A–Sn1A–Cl1A	169.33(3)	N1B–Sn1B–Cl1B	170.40(4)
N1A–Sn1A–C11A	75.01(6)	N1B–Sn1B–C11B	75.24(6)
N1A–Sn1A–C12A	91.72(6)	N1B–Sn1B–C12B	91.89(6)
N1A–Sn1A–C18A	90.31(6)	N1B–Sn1B–C18B	89.02(6)
C11A–Sn1A–ClA	94.36(5)	C11B–Sn1B–ClB	95.55(5)
C12A–Sn1A–ClA	94.70(5)	C12B–Sn1B–ClB	94.97(5)
Bond Lengths of 10 (Å)		**Bond Lengths of 11 (Å)**	
Sn1–N1	2.383(3)	Sn1–N1	2.4245(18)
Sn1–C1	2.137(2)	Sn1–C1	2.127(2)
Sn1–C12	2.127(2)	Sn1–C13	2.1302(19)
Sn1–Br1	2.4943(3)	Sn1–Br1	2.5167(3)
Sn1–Br2	2.6180(3)	Sn1–Br2	2.6394(3)

Table 2. *Cont.*

Bond Angles of 10 (°)		Bond Angles of 11 (°)	
N1–Sn1–Br2	171.36(5)	N1–Sn1–Br2	84.68(4)
N1–Sn1–Br1	87.98(5)	N1–Sn1–Br1	172.89(4)
N1–Sn1–C1	76.06(6)	N1–Sn1–C1	78.24(8)
N1–Sn1–C12	89.86(8)	N1–Sn1–C13	95.47(8)
C12–Sn1–C1	126.73(9)	C1–Sn1–C13	136.53(8)
Br1–Sn1–Br2	91.994(11)	Br1–Sn1–Br2	91.148(9)

The geometry around the Sn centers of **10** (τ_5 = 0.74) and **11** (τ_5 = 0.89) are also distorted trigonal bipyramidal as described previously. Possible evidence for a 3c–4e$^-$ sharing is given by the relatively short Sn1–N1 bond lengths and the elongated apical Sn1–Br2 (**10**) interaction and the corresponding Sn1–Br1 (**11**) bond distances (Table 2), compared to average covalent Sn–Br bond lengths (≈2.56 Å) [34]. The electron withdrawing effect of the apical bromine atom in **10** and **11** appears to draw the nitrogen closer to the tin center, resulting in a short Sn–N bond length of 2.383(3) Å for **10**, and a slightly longer bond length in **11**. For comparison, Novák et al. [37] and Švec and co-workers [38] independently reported related hypercoordinate phenyldichlorido and phenyldiiodidotin structures possessing a chelating benzyl amine substituent (Figure 1). These compounds display Sn–N bond distances of 2.444(5) Å and 2.476(3) Å, which are ≈0.06 and 0.04 Å longer than that of **10** and **11**, respectively.

2.3. DFT Studies

The seven crystallographically determined structures in this study (compounds **4** (**4′**,**4″**), **7**, **9** (**9′**,**9″**), **10**, **11**) provide a small structurally-related dataset to compare with DFT models. We have previously summarized the problematic aspects of comparing calculated and experimental structural data [17]; nevertheless, it remains a useful approach for refining a DFT description of these hypercoordinate systems. Previous work has demonstrated that the LANL08d ECP for Sn and Br, and 6-31+G(d,p) for all other atoms provide accurate structures at moderate computational cost [39,40]. In a recent evaluation of selected density functionals, we found that B3PW91 [41] and PBE0 "PBE1PBE" [42] when supplemented with Grimme's D3 empirical dispersion function and Becke-Johnson damping (GD3BJ) [43] outperformed eight other methods in predicting hypercoordinate Sn geometries [17]. The use of diffuse functions on non-H atoms significantly improved accuracy as did augmenting methods with empirical dispersion. This latter finding was also reported in a recent comprehensive study [44], which included among its recommendations that M052X-GD3 [45,46] was effective for modelling general main-group thermochemistry, kinetics, and non-covalent interactions.

Experimental and calculated structures were compared by aligning them to maximize overlap. The central Sn atoms for the two structures were superimposed and then one structure was rotated relative to the other to minimize the mean sum of squared distances (MSSDs) between equivalent heavy (non-H) atoms on the two structures. Since the position of the Sn atoms is fixed, Sn is excluded from the average. The MSSD is a demanding metric for assessing accuracy of a calculated structure. Alignment of the experimental and calculated structures causes differences in bond lengths and angles at the Sn center to be propagated throughout the structure, increasing the distances between equivalent atoms at multiple locations. Small deviations are thus amplified, leading to larger mean values and greater discrimination between models for calculated structures. At the same time, the MSSD is acutely sensitive to small displacements in dihedral angles for phenyl ligands or any solid-state structural distortions due to packing forces or intermolecular associations between Sn atoms. To minimize the impact of phenyl ligand dihedral differences, only the Ph-C atoms directly bonded to Sn were included in the MSSD calculations.

Table 3 shows the MSSD values determined for structures calculated by the three DFT methods for the seven compounds in this study. The largest MSSDs are found for **4** and **11**, both compounds

that contain an additional –CH_2– bridge resulting in a twisted six-member hypercoordination ring, rather than the nearly planar five-member ring of the other compounds. The additional flexibility in these structures may allow for greater distortions in the solid state. Compound **11** is unique in the series in having a planar oxazoline ring in the solid state. All other structurally characterized compounds, and all calculated structures display a slight pucker in the oxazoline groups. Energy differences between planar and puckered oxazoline ring conformations are expected to be small enough to allow for stabilization of the higher energy conformer by packing forces. In the case of **10**, observed crystallographic disorder is consistent with the presence of two oxazoline ring twist isomers that are resolvable due to the Sn hypercoordination. The MSSDs observed for **7**, **9**, and **10** are comparable with those measured for Sn complexes with phenyl ligands in the previous study [17]. In all cases, there is evidence of some distortion in the solid-state structures, typically seen in the bending of a phenyl ligand at the coordinating C atom, such that the Sn–C(Ph) bond no longer lies in the plane of the phenyl ring.

Table 3. Minimized mean sum of squared distances (MSSDs) between equivalent heavy (non-H) atoms in calculated and experimental molecular structures.

Compound	B3PW91-GD3BJ	PBE0-GD3BJ	M05-2X-GD3
4′ [a,b]	0.204	0.186	0.188
4″ [a,b]	0.223	0.200	0.198
7 [c]	0.0104	0.00757	0.0120
9′ [a,d]	0.0229	0.0208	0.0206
9″ [a,d]	0.0332	0.0331	0.0335
10 [e]	0.0191	0.0141	0.0151
11	0.0526	0.0572	0.0792

[a] Compound has two crystallographically-independent conformers in unit cell. [b] 17 of 32 non-H atoms. [c] 16 of 31 non-H atoms. [d] 16 of 26 non-H atoms. [e] 16 of 21 non-H atoms; oxazoline ring has some disorder, atoms O1A and C8A were used in calculations.

The three DFT methods perform very similarly by the MSSD measure for this series of compounds. Since B3PW91-GD3BJ and PBE0-GD3BJ were among the best functionals considered in the earlier study, [17] this suggests that M05-2X-GD3 is also a good choice for modelling hypercoordinate Sn compounds. The substantial similarity in the results for the three calculation methods suggests that the treatment of dispersion is the dominant factor in overall predictive accuracy, minimizing differences in the quality of performance of the hybrid functionals. Overall, for this limited series of compounds, PBE0-GD3BJ slightly outperformed the other two methods. It is interesting to compare the performance in predicting individual bonds and angles. In most cases (**4′**, **4″**, **7**, **9′**, **9″**), M05-2X-GD3 resulted in the smallest mean unsigned error (MUE) in the Sn–N separation distances; B3PW91-GD3BJ produced smaller MUEs for **10** and **11**. The Sn–C(Ar) bond MUE was most often smallest for PBE0-GD3BJ (**4′**, **4″**, **7**, **10**, **11**). Overall, M05-2X-GD3 provided better estimates of bond angles at the Sn center. The differences in performance for different bond and angle types is a typical complication of structural benchmarking studies, as is the requirement to average measures across a series of compounds. One of the advantages of the MSSD is that it combines the effects of all bond and angle estimates into one comprehensive measure that can be applied to an individual compound rather than an extended series. This makes it easier to pool observations from earlier studies as well as to evaluate new compounds not previously considered.

2.4. Oxazoline Stannane Dihydrides

The synthesis of dihydride **12** was successfully achieved using 1.5 mol equivalent of $NaBH_4$ in EtOH, at −84 °C for 1 h from **10**; albeit in relatively low yield (43%).

Compound **12** was initially isolated as a colourless viscous oil and requires cooling (−84 °C) to retard decomposition. Staliński et al. had also reported an analogous chiral stannane, **2h** (Figure 2), shows sensitivity above −20 °C [30]. The thermal sensitivity of **12** was evident when a NMR sample of the compound was quickly (~1 min) prepared in C_6D_6; the solution rapidly changes from colourless to a bright yellow coloured solution, with a precipitate being noted within a few hours. The ^{1}H NMR spectrum of clean **12** (Figure S24) shows a singlet at 6.79 ppm with distinct $^{117/119}$Sn satellites (^1J ^{117}Sn–H = 1938 Hz, ^1J ^{119}Sn–H = 2028 Hz). These resonances and coupling constants are comparable to other tin hydrides, including **2h** [30]. The ^{119}Sn NMR of **12** reveals a single resonance at −249.5 ppm, (Figure 7, t = 0) similar to that reported for **2g** (δ_{117Sn} = −244.5 ppm in toluene-d_8). Five coordinate tin dihydrides bearing 'flexible' ligands give typical ^{119}Sn shift values between −200 and −220 ppm. The upfield shift of **12** relative to these latter stannanes may be a consequence of the close proximately of the nitrogen to the tin center. To investigate the stability of these dihydrides, ^{119}Sn NMR spectrum of an initial solution of clean **12** were collected consecutively for 13 h (Figure 6). After 2 h, the appearance of two new signals (−42 and −173 ppm) was detected. After 8 h, all of **12** had been consumed. The NMR tube was then protected from light using Al foil and the contents re-examined after 7d. The ^{119}Sn NMR spectrum revealed the disappearance of the resonances at −42 and −173 ppm and the appearance of multiple new unidentified resonances, as shown below (Figure 7).

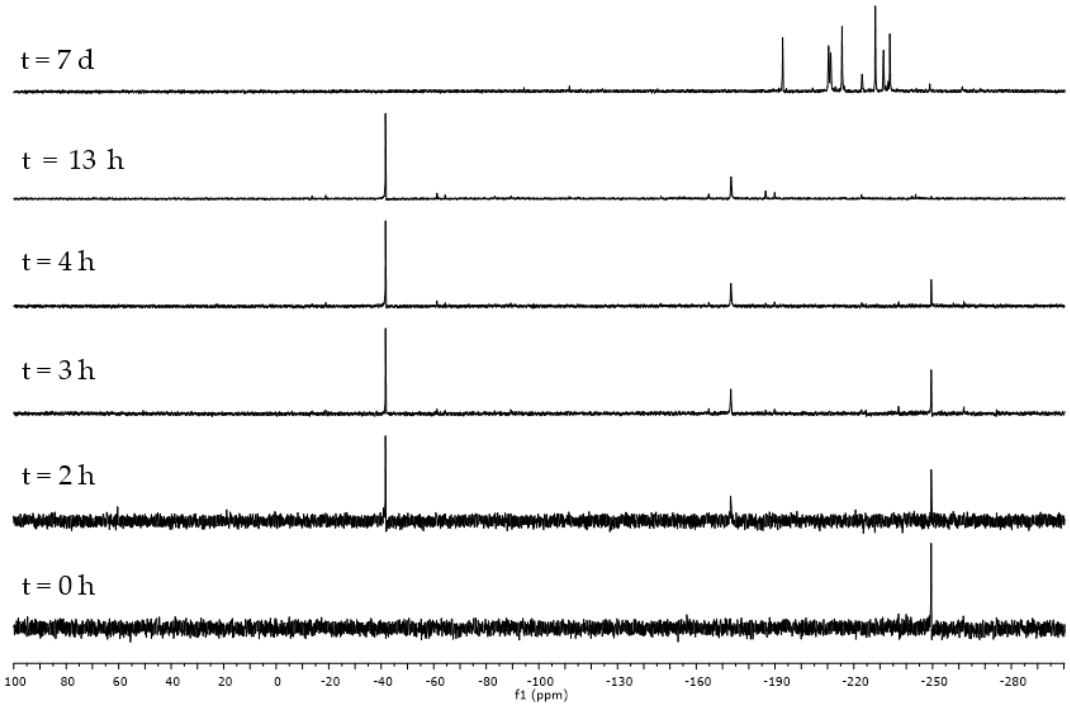

Figure 7. Time dependent ^{119}Sn NMR spectra (C_6D_6) of **12** at 27 °C.

Compound **13** (Scheme 5) was prepared via a traditional transformation of **11** using a large excess of $NaBH_4$ in EtOH for 1 h at 0 °C. After work-up, a colourless viscous oil was recovered (86%). Compound **13**, like **12**, turned yellow in colour when dissolved in C_6D_6; however, clean NMR analysis was still possible. In the ^{1}H NMR spectrum (Figure S49), the Sn–H signal appears at δ_{1H} = 5.94 ppm with appropriate $^{117/119}$Sn satellites. A single resonance (δ = −221.0 ppm) was observed in the ^{119}Sn NMR spectrum for **13**, this is ≈30 ppm downfield relative to that of **12**.

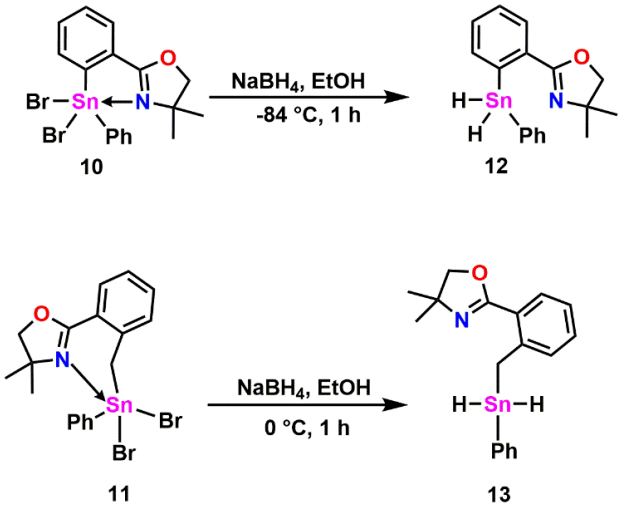

10 12 11 13

Scheme 5. Preparation of tin dihydrides **12** and **13**.

2.5. Synthesis of Polymers *14* and *15*

It has been previously shown that Wilkinson's catalyst is ineffective for the polymerization of diaryl tin hydrides [47]. However, more recent reports have demonstrated that this catalyst is effective with mixed aryl/alkyl tin dihydrides that contain other donor atoms with potential to bind to Sn [7,8,48]. As a consequence of the thermal/solution sensitivity of monomers **12** and **13**, dehydropolymerization attempts were carried out immediately after their preparation. Such polymerizations are often performed at RT in toluene; however, a temperature of 0 °C was selected (Scheme 6) to offset the rapid decomposition/oligomerization of these monomers prior to interaction with the catalyst.

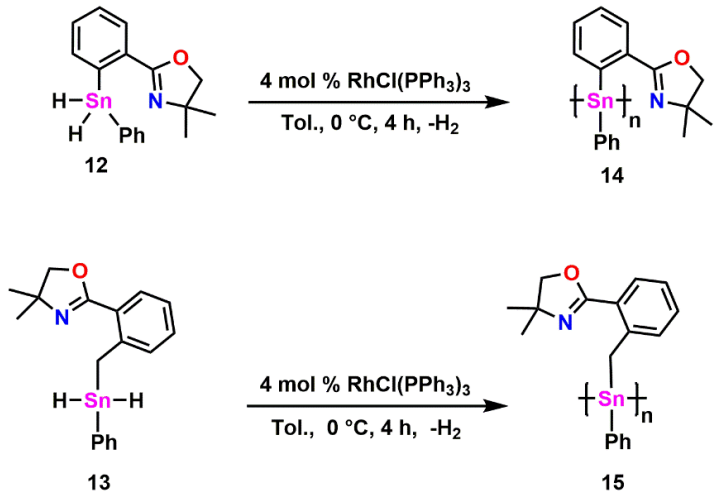

12 14 13 15

Scheme 6. Preparation of tin oxazoline polymers **14** and **15**.

The recovered crude yellow coloured polymer mixture was cleaned by repeated re-precipitation of THF solution mixture (2 mL) being deposited into cold stirring hexanes (3 × 75 mL) and heptane (1 × 75 mL). A pale-yellow powder of **14** was recovered, which reveals a single, broad ^{119}Sn resonance (δ = −268.1 ppm). This value is ≈20 ppm upfield shift relative to that of **12**. The ^{1}H NMR spectrum showed the disappearance of the Sn–H signal (δ = 6.79 ppm) and a broadening of the other resonances, all characteristic of polymer formation. Unfortunately, repeated precipitation did not completely remove all of the impurities as identified by NMR spectroscopy. Gel permeation chromatography (GPC) was performed to estimate the molecular weight of **14**, which shows a bimodal distribution (Figure 8 red). A molecular weight determination revealed that the polymer was of low M_w (≈ 10,100 Da) with a $Đ$ of 1.73. This corresponds to short polymer chains with ≈27 repeat units.

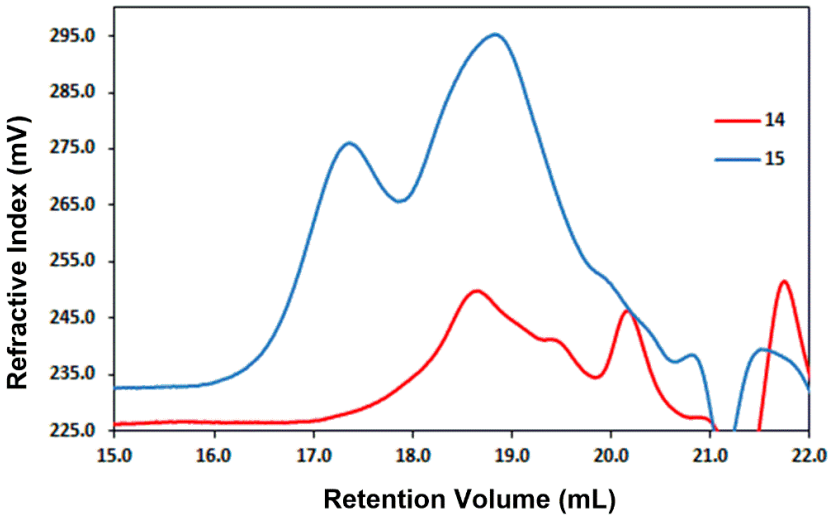

Figure 8. GPC chromatograms of polystannanes **14** (red) and **15** (blue).

Dehydropolymerization of **13** (Scheme 6) at 0 °C in toluene in the presence of Wilkinson's catalyst yielded a yellow coloured powder after work up. A preliminary ^{119}Sn NMR analysis of the reaction mixture showed five tin resonances in the crude NMR spectrum (Figure 9a). The crude polymer **15** was cleaned in a manner similar to **14** resulting in the isolation of a pale-yellow coloured powder, which showed a single downfield resonance by NMR spectroscopy (δ_{119Sn} = −183.8 ppm, Figure 9b) but contained other organic impurities, as identified by ^{1}H NMR. This unexpected downfield chemical shift suggests that the oxazoline substituent may not be coordinating to the tin center in this product [7,8]. GPC analysis of **15** revealed again bimodal behaviour (Figure 8, blue: Peak 1: M_w = 15,400 Da, $Đ$ = 1.03, Peak 2: M_w = 24,400 Da, $Đ$ = 1.82). After additional cleaning, a bimodal distribution was still observed and a lower molecular weight detected (Peaks 1 and 2: M_w = 3200 Da and $Đ$ of 1.56). This corresponds to ≈7 units and suggests that **15** may experience some degree of polymer degradation or that it is essentially oligomeric in nature. Unfortunately, due to the low molecular weights and low purity (NMR) obtained for polymers **14** and **15**, other meaningful polymer analysis, including EA, were not performed.

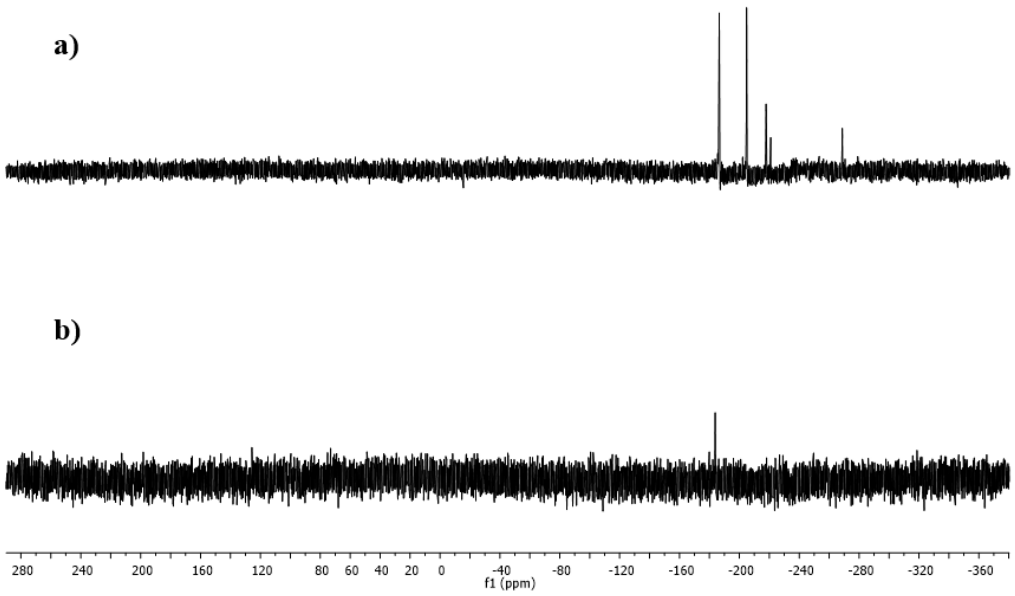

Figure 9. Crude (**a**) and clean (**b**) ^{119}Sn NMR (C_6D_6) spectrum of **15**.

3. Materials and Methods

3.1. General Considerations

All reagents and solvents were obtained from Sigma-Aldrich (Oakville, Canada) and used as received, unless otherwise indicated. Solvents were dried either through an MBraun solvent drying system, or through vacuum distillation and stored under an inert nitrogen atmosphere. All reactions were carried out under nitrogen atmosphere using Schlenk techniques, unless otherwise noted. ^{1}H NMR (400 MHz), ^{13}C NMR (100.6 MHz), and ^{119}Sn NMR (149.2 MHz) spectra were recorded on a Bruker Avance 400 NMR spectrometer (Bruker Corporation, Billerica, MA, USA) with a BBFO 5-mm direct probe. A ^{1}H pulse width of 30° was used, acquiring a spectral window of 8223 Hz (20 ppm) using a relaxation delay of 1s, acquisition time 3.98 s, 32 k points (16 scans). The ^{1}H 90° pulse width was 10.4 µs. A ^{13}C pulse width of 30° was used, acquiring a spectral window of 24,038 Hz (239 ppm) using a relaxation delay of 2 s, acquisition time 1.36 s, 32 k points (4096 scans). The ^{13}C 90° pulse width was 8.7 µs. A ^{119}Sn pulse width of 30° was used, 8.75 µs, acquiring a spectral window of 100,000 Hz (670 ppm) using a relaxation delay of 1s, acquisition time 0.33 s, 32 k points (15,360 scans) with inverse gated proton decoupling. All results were analysed on MestReNova LITE 5.2.5 software (Mestrelab Research, S. L., Santiago Compostelea, Spain). Chemical shifts were calculated using the chemical deuterated standards as a reference for ^{1}H and ^{13}C. The ^{119}Sn chemical shifts were referenced to $SnMe_4$ as an external standard. All *J* coupling values are reported as absolute values. All NMR assignments of small molecules were made using 2D NMR spectroscopy (COSY, HMBC, HSQC) experiments. Time-of-flight mass spectrometry analyses were performed at the AIMS Mass Spectrometry Laboratory, University of Toronto using a JMS-T1000LC mass spectrometer (JEOL, Inc., Peabody, MA, USA) equipped with a Direct Analysis in Real Time (DART) ionization source (DART-SVP, Ionsense, Inc., Saugus, MA, USA). The DART source was operated with He gas and the temperature was adjusted in the range 100–400 °C. Isotopic distributions for the observed ionic species were calculated using the Mass Center utility (JEOL) and were in good agreement with the measured mass spectra. Molecular weights of the polymers were determined by GPC using a Viscotek Triple Model 302 Detector system. GPC columns were calibrated versus polystyrene standards (American Polymer Standards). A flow rate of 1.0 mL/min was used with ACS grade THF as the eluent. GPC samples were prepared using 3–10 mg of each polymer per mL THF, and filtered using a 0.45 µm filter. All reactions were carried out under a nitrogen atmosphere using Schlenk techniques, unless otherwise described. The X-ray diffraction data for single crystals of compounds **4**, **7**, **9**, **10**, and **11** were collected on a Bruker Kappa APEX-DUO diffractometer using monochromated Mo-Kα radiation (Bruker Triumph) and were measured using a combination of ϕ scans and ω scans (Table 4). The data were processed using APEX2 and SAINT programs. Absorption corrections were carried out using SADAB. The structures were solved using SHELXT [49] and refined using SHELXL-2013 [49] for full-matrix least-squares refinement that was based on F^2. For all structures, H atoms were included in calculated positions and allowed to refine in a riding-motion approximation with U_{iso} tied to the carrier atom.

Table 4. Crystal data and structure refinement of complexes **4**, **7**, **9** –**11**.

Complexes	4	7	9	10	11
CCDC number	1987221	1987224	1987220	1987222	1987223
Empirical Formula	$C_{30}H_{29}NOSn$	$C_{29}H_{27}NOSn$	$C_{23}H_{22}ClNOSn$	$C_{17}H_{17}Br_2NOSn$	$C_{18}H_{19}Br_2NOSn$
Formula Weight	538.23	524.20	482.55	529.82	543.85
Crystal System	Orthorhombic	Monoclinic	Triclinic	Monoclinic	Triclinic
Space Group	$P2_12_12_1$	$P2_1/n$	P−1	$P2_1/n$	P−1
α/Å	8.4502(2)	9.3351(5)	9.1303(4)	10.5295(7)	8.4530(5)
b/Å	18.9557(5)	18.4709(9)	9.3020(4)	10.0336(5)	10.2368(5)
c/Å	31.5231(9)	14.3598(7)	24.2461(11)	17.1396(11)	11.7987(7)
α/°	90	90	90.942(1)	90	93.059(2)
β/°	90	93.8460(10)	91.775(1)	96.667(2)	101.936(2)
γ/°	90	90	91.724(1)	90	108.325(2)
V/Å^3	5049.4(2)	2470.5(2)	2056.99(16)	1798.50(19)	940.50(9)
Z	8	8	4	4	2
D_{calc}/g cm^{-3}	1.416	1.409	1.558	1.957	1.920
μ (Mo Kα)/Å	0.71073	0.71073	0.71073	0.71073	0.71073
Temperature/°K	150(2)	150(2)	150(2)	150(2)	150(2)
θ range, °	1.680–27.489	1.799–27.517	0.840–27.599	2.164–27.535	1.779–27.500
Reflections collected	27514	39843	66519	38637	43074
Unique reflections	11499	5684	9482	4135	4285
R_{int}	0.0346	0.0229	0.0237	0.0237	0.0304
Residuals: R_1 ($I > 2\ \sigma\ (I)$)	0.0316	0.0212	0.0205	0.0219	0.0183
Residuals: *R* (All reflections)	0.0449	0.0281	0.0255	0.0358	0.0250
Residuals: wR_2 (All reflections)	0.0517	0.0452	0.0413	0.0422	0.0387
Goodness of fit indicator	0.987	1.105	1.096	1.052	1.115
Max/min peak,/e Å^{-3}	0.473/−0.414	0.542/−0.459	0.429/−0.600	0.553/−0.467	0.542/−494

$R_1 = \Sigma\ ||Fo| - |Fc||/\Sigma\ |Fo|$, $wR_2 = [\Sigma\ (w(Fo^2 - Fc^2)^2)/\Sigma\ w(Fo^2)^2]^{1/2}$.

3.2. Computational Details

The Gaussian 16 suite of programs was used for all geometric optimizations and frequency calculations [50]. DFT was implemented with three density functionals (B3PW91, PBE1PBE, and M05-2X) supplemented with Grimme's D3 empirical dispersion function and for B3PW91 and PBE1PBE, Becke-Johnson damping [43]. The LANL08d basis set (obtained from the Basis Set Exchange) [51] was used for Sn and Br, and the 6-31+G(d,p) basis set for all other atoms, as a reasonable compromise between accuracy and computational cost [39,40]. Tight convergence criteria and the superfine integration grid was used for all geometry optimizations. Frequency calculations were used in every case to verify that a potential energy minimum had been located. Cartesian coordinates for experimental structures were extracted from crystallographic information files (.cif) with OpenBabelGUI [52].

3.3. Synthesis of 2-(2-Bromophenyl)-4,4-dimethyl-4,5-dihydrooxazole (**5**)

Method 1: Thionyl chloride (3.60 mL, 49.8 mmol) and 3 drops of DMF were added to a 250 mL round bottom flask containing 2-bromobenzoic acid (5.00 g, 24.9 mmol) in 100 mL of dry DCM. The reaction mixture was heated to reflux temperature for 2 h. The solvent and excess thionyl chloride were then removed under reduced pressure to afford a yellow coloured liquid. The product was dissolved in 30 mL of dry DCM and then added dropwise to a 250 mL round bottom flask containing a stirring solution of distilled 2-amino-2-methyl-1-propanol (2.66 g, 29.9 mmol) and NEt_3 (5.20 mL, 37.3 mmol) in 100 mL of dry DCM at 0 °C. The reaction mixture was then stirred for 4 h at RT. The crude sample was washed once with 30 mL of 1 M solution of aqueous HCl and 2 × 30 mL of a saturated aqueous brine solution. The organic layer was then dried over anhydrous $MgSO_4$, filtered, and the solvent removed under reduced pressure to afford 2-bromo-*N*-(1-hydroxy-2-methylpropan-2-yl)benzamide as a white coloured powder in a 82.0% yield. The benzamide (5.55 g, 20.4 mol) was dissolved in $SOCl_2$ (15.0 mL, 206 mmol) at 0 °C. The solution was stirred at RT for 24 h, after which 100 mL of Et_2O was added and the precipitate collected via vacuum filtration and dissolved in 50 mL of DCM. The DCM mixture was washed with a saturated aqueous solution of $NaHCO_3$ until the organic layer was neutral and then

dried over anhydrous $MgSO_4$. After filtration, the solvent was removed under reduced pressure to yield 2-(2-bromophenyl)-4,4-dimethyl-2-oxazoline, **5**, as a white coloured powder. Yield: 4.75 g, 75.2%. NMR data (^{1}H, ^{13}C) matches reported literature data within experimental error [53].

Method 2: A solution containing 2-bromobenzonitrile (0.50 g, 2.75 mmol), 2-amino-2-methyl-1-propanol (0.37 g, 4.12 mmol) and anhydrous $ZnCl_2$ (0.037 g, 0.27 mmol) were heated to reflux temperature in 15 mL of chlorobenzene for 24 h. The solvent was then removed under reduced pressure. The crude product was purified via flash chromatography (EtOAc/Hex (1:1)) to yield 2-(2-bromophenyl)-4,4-dimethyl-2-oxazoline, **5**, as a white coloured powder. Yield: 0.52 g, 74.2%. m.p. 39–40 °C (Literature: 36–38 °C) NMR data (^{1}H, ^{13}C) matches reported literature data within experimental error [54]. ^{1}H NMR (400.13 MHz, $CDCl_3$, δ): 7.66 (dd, 1H, H6, $^3J_{1H–1H}$ = 7.8 Hz, $^4J_{1H–1H}$ = 1.5 Hz), 7.63 (dd, 1H, H9, $^3J_{1H–1H}$ = 7.8 Hz, $^4J_{1H–1H}$ = 1.4 Hz), 7.34 (td, 1H, H7, $^3J_{1H–1H}$ = 7.5 Hz, $^4J_{1H–1H}$ = 1.4 Hz), 7.28 (td, 1H, H8, $^3J_{1H–1H}$ = 7.5 Hz, $^4J_{1H–1H}$ = 1.8 Hz), 4.16 (s, 2H, H3), 1.43 (s, 6H, H1) ppm. ^{13}C{^{1}H} NMR (100.61 MHz, $CDCl_3$, δ): 161.79 (C4), 133.59 (C9), 131.56 (C8), 131.26 (C6), 130.27 (C10), 127.07 (C7), 121.82 (C5), 79.44 (C3), 68.05 (C2), 28.25 (C1) ppm.

*3.4. Synthesis of 4,4-Dimethyl-2-(2-(triphenylstannyl)phenyl)-4,5-dihydrooxazole (**7**):*

Method 1: Compound **5** (0.565 g, 2.22 mmol) and 15 mL of dry Et_2O were added to a dry 100 mL Schlenk flask. The solution was cooled to −84 °C and 1.6 M *n*-BuLi/hexane (1.52 mL, 2.45 mmol) was added dropwise. The reaction mixture was stirred for 2 h at −84 °C, and then was allowed to warm to 0 °C before the dropwise addition of a solution containing Ph_3SnCl (0.857 g, 2.22 mmol) in 20 mL of Et_2O. The reaction mixture was stirred for 1 h at 0 °C. The solvent was removed under reduced pressure and 20 mL of toluene was added. The mixture was filtered via gravity filtration and the solvent was removed under reduced pressure to yield a pale yellow coloured powder. The crude product was triturated with MeOH and the yellow supernatant decanted from the solid. The residual solvent was removed under reduced pressure to yield **7** as a white coloured powder. Yield: 0.86 g, 73.9%.

Method 2: Compound **6** (5.00 g, 28.5 mmol) and 50 mL of dry Et_2O were added to a dry 250 mL Schlenk flask. The solution was cooled to −84 °C and 1.3 M *sec*-BuLi/cyclohexane (24.14 mL, 31.39 mmol) was added dropwise. The reaction mixture stirred for 1.5 h at −84 °C and then allowed to warm to 0 °C before the dropwise addition of a solution of Ph_3SnCl (11.0 g, 28.5 mmol) in 20 mL of Et_2O. The reaction mixture was stirred for 1 h at 0 °C. The solvent was then removed under reduced pressure and 40 mL of toluene was added. The mixture was filtered via gravity filtration and the solvent removed under reduced pressure to yield a pale yellow coloured powder. The crude product was triturated with MeOH and the yellow supernatant decanted from the solid. The residual solvent was removed under reduced pressure to yield **7** as a white coloured powder. Recrystallization was achieved by dissolving the powder (0.5 g) in DCM (1 mL) and layering with hexanes (1.5 mL). The sample was cooled to −20 °C overnight to yield clear colourless crystals of **7**. Yield: 11.42 g, 76.3%. m.p. 139–141 °C. ^{1}H NMR (400.13, $CDCl_3$, δ): 8.05 (d, 1H, H9, $^3J_{1H–1H}$ = 7.8 Hz, $^3J_{1H–119/117Sn}$ = 24.6 Hz), 7.61–7.59 (m, 6H, H12), 7.54–7.52 (m, 1H, H6), 7.50–7.48 (m, 1H, H7), 7.45–7.42 (m, 1H, H8), 7.36–7.34 (m, 9H, H13 & H14), 3.93 (s, 2H, H3), 0.77 (s, 6H, H1) ppm. ^{13}C {^{1}H} NMR (100.61 MHz, $CDCl_3$, δ): 163.19 (C4), 143.19 (C11), 141.28 (C10), 138.71 (C6), 137.11 (C13, $^3J_{13C–117/119Sn}$ = 37.4 Hz), 133.71 (C5), 131.02 (C8), 129.08 (C7), 128.10 (C14), 128.04 (C12), 127.80 (C9), 80.05 (C3), 67.49 (C2), 27.62 (C1) ppm. ^{119}Sn {^{1}H} NMR (149.21 MHz, $CDCl_3$, δ): −157.13 ppm. HRMS-DART (*m*/*z*) = 448.07234 [M − C_6H_5] calculated for $^{12}C_{23}{}^1H_{22}{}^{14}N_1{}^{16}O_1{}^{120}Sn_1$; found 448.07136.

*3.5. Synthesis of 2-(2-(Chlorodiphenylstannyl)phenyl)-4,4-dimethyl-4,5-dihydrooxazole (**9**)*

Compound **7** (0.250 g, 0.477 mmol) and 10 mL of C_6H_6 were added to a dry 100 mL Schlenk flask. A 1.0 M HCl/Et_2O solution (0.47 mL, 0.477 mmol) was added and the mixture stirred for 1 h at RT. The solvent was removed under reduced pressure, and the crude product triturated with hexanes. The cloudy supernatant was removed from the solid and residual solvent removed under reduced pressure to afford **9** as a white coloured powder. Recrystallization of **9** (0.100 g) was achieved by

dissolving the powder in a minimal amount of DCM (0.2 mL) and layering with hexanes (0.5 mL), followed by cooling to −20 °C overnight, yielding clear colourless crystals. Yield: 0.192 g, 83.6%. m.p: 222–223 °C. ^{1}H NMR (400.13, $CDCl_3$, δ): 8.57 (d, 1H, H9, $^{3}J_{1H–1H}$ = 7.0 Hz, $^{3}J_{1H–117Sn}$ = 60.1 Hz, $^{3}J_{1H–119Sn}$ = 74.5 Hz), 7.95 (d, 1H, H6, $^{3}J_{1H–1H}$ = 7.5 Hz), 7.79–7.75 (m, 1H, H8), 7.74–7.71 (m, 4H, H12), 7.63–7.61 (m, 1H, H7), 7.39–7.37 (m, 6H, H13 & H14), 4.27 (s, 2H, H3), 0.86 (s, 6H, H1) ppm. ^{13}C {^{1}H} NMR (100.61 MHz, $CDCl_3$, δ): 168.90 (C4), 143.23 (C11), 143.02 (C10), 138.42 (C9), 135.62 (C13, $^{3}J_{13C–117/119Sn}$ = 47.7 Hz), 133.25 (C8), 130.76 (C5), 130.01 (C7), 129.25 (C14, $^{4}J_{13C–117/119Sn}$ = 15.4 Hz), 128.55 (C12, $^{2}J_{13C–117/119Sn}$ = 75.6 Hz), 126.76 (C6), 82.58 (C3), 66.91 (C2), 27.73 (C1) ppm. ^{119}Sn {^{1}H} NMR (149.21 MHz, $CDCl_3$, δ): −226.0 ppm.

*3.6. Synthesis of 2-(2-(Dibromo(phenyl)stannyl)phenyl)-4,4-dimethyl-4,5-dihydrooxazole (**10**)*

Compound **7** (8.224 g, 15.69 mmol) and 50 mL of C_6H_6 were added to a 250 mL Schlenk flask and cooled to 0 °C. Br_2 (1.61 mL, 31.45 mmol) was added dropwise and the reaction mixture stirred for 1 h. The solvent was removed under reduced pressure to yield a brown-yellow coloured powder. The crude product was triturated with MeOH and the yellow supernatant removed from the solid. The residual solvent was removed under reduced pressure to afford the product, **10**, as a white coloured powder. Recrystallization of **10** (0.500 g) was achieved by dissolving the powder in a minimal amount of DCM (0.5 mL) and layering with ether (0.5 mL). Overnight cooling (−20 °C) yielded clear colourless crystals. Yield = 6.60 g, 79.4%. m.p. 197–198 °C. ^{1}H NMR (400.13, $CDCl_3$, δ): 8.51 (d, 1H, H9, $^{3}J_{1H–1H}$ = 7.3 Hz, $^{3}J_{1H–117Sn}$ = 86.3 Hz, $^{3}J_{1H–119Sn}$ = 101.4 Hz), 7.92 (d, 1H, H6, $^{3}J_{1H–1H}$ = 7.5 Hz), 7.81 (td, 1H, H8, $^{3}J_{1H–1H}$ = 7.5 Hz, $^{4}J_{1H–1H}$ = 1.5 Hz), 7.68–7.63 (m, 3H, H7 & H12), 7.45–7.38 (m, 3H, H13 & H14), 4.38 (s, 2H, H3), 1.15 (s, 6H, H1) ppm. ^{13}C {^{1}H} NMR (100.61 MHz, $CDCl_3$, δ): 168.52 (C4), 144.62 (C11), 140.58 (C10), 137.81 (C9, $^{2}J_{13C–117/119Sn}$ = 58.4 Hz), 133.88 (C7), 133.34 (C13, $^{3}J_{13C–117/119Sn}$ = 68.2 Hz), 131.41 (C8, $^{3}J_{13C–117/119Sn}$ = 15.3 Hz), 130.20 (C14, $^{4}J_{13C–117/119Sn}$ = 20.5 Hz), 129.16 (C5), 129.01 (C12, $^{2}J_{13C–117Sn}$ = 96.8 Hz, $^{2}J_{13C–119Sn}$ = 101.2 Hz), 126.95 (C6), 83.7 (C3), 67.09 (C2), 27.98 (C1) ppm ^{119}Sn {^{1}H} NMR (149.21 MHz, $CDCl_3$, δ): −290.63 ppm. HRMS-DART (*m*/*z*): [M^+] calculated for $^{12}C_{17}{}^{1}H_{18}{}^{79}Br_2{}^{14}N_1{}^{16}O_1{}^{120}Sn_1$: 529.87771; found 529.87682.

*3.7. Synthesis of 4,4-Dimethyl-2-(2-(phenylstannyl)phenyl)-4,5-dihydrooxazole (**12**)*

A suspension of **11** (0.50 g, 0.94 mmol) in 15 mL of dry EtOH was added dropwise to a solution of $NaBH_4$ (0.053 g, 1.42 mmol) in 5 mL of dry EtOH at −84 °C. The solution was stirred at −84 °C for 1 h. Cold hexane (15 mL) was added to the solution and then quenched with 5 mL of chilled degassed distilled water. The mixture was extracted and the organic layer dried over anhydrous $MgSO_4$. The solution was filtered and the solvent was removed under reduced pressure to yield the product **12** as a colourless viscous oil. Yield = 0.151 g, 43%. ^{1}H NMR (400.13, C_6D_6, δ): 8.01–7.99 (m, 1H, H6), 7.77–7.75 (m, 1H, H9), 7.70–7.68 (m, 1H, H7), 7.21–7.18 (m, 3H, H14 & H15), 7.15–7.14 (m, 1H, H8), 7.12–7.08 (m, 2H, H13), 6.79 (s, H, H11, $^{1}J_{1H–117Sn}$ = 1938 Hz, $^{2}J_{1H–119Sn}$ = 2028 Hz), 3.59 (s, 2H, H3), 0.98 (s, 6H, 1H) ppm. ^{13}C {^{1}H} NMR (100.61 MHz, C_6D_6, δ): 164.22 (C4), 141.60 (C10) 141.56 (C12), 138.68 (C9), 137.28 (C13), 137.21 (C5), 133.21 (C7), 130.97 (C8), 128.88 (C14), 128.15 (C15), 128.03(C6), 79.82 (C3), 67.07 (C2), 28.28 (C1) ppm. ^{119}Sn {^{1}H} NMR (149.21 MHz, C_6D_6, δ): −249.5 ppm. HRMS-DART (*m*/*z*): [M − H] calculated for $^{12}C_{17}{}^{1}H_{18}{}^{14}N_1{}^{16}O_1{}^{120}Sn_1$: 372.04451; found 372.04104.

*3.8. Synthesis of Polymer (**14**)*

A solution of **12** (0.327 g, 0.879 mmol) in 3 mL of dry toluene was added dropwise to a dry Schlenk wrapped in Al foil containing Wilkinson's catalyst (0.033 g, 0.035 mmol) in 10 mL of dry toluene at 0 °C. The solution was stirred at 0 °C for 4 h, after which the solvent was removed under reduced pressure. The crude product was dissolved in minimal dry THF (2 mL) and added dropwise to cold stirring hexanes (3 × 75 mL) and heptane (1 × 75 mL), and the residual solvent removed under reduced pressure to yield a pale-yellow powder of **14**. Yield = 0.052 g, 15.9%. ^{1}H NMR (400.13, C_6D_6, δ):

7.74–7.69 (m, 4H), 7.09–7.00 (m, 5H), 3.57 (m, 2H). Note: The methyl resonances were obscured by the presence of solvent and not assigned. ^{119}Sn {^{1}H} NMR (149.21 MHz, C_6D_6, δ): −268.1 ppm.

*3.9. Synthesis of 4,4-Dimethyl-2-(o-tolyl)-4,5-dihydrooxazole (**8**)*

Thionyl chloride (5.35 mL, 73.4 mmol) and 3 drops of DMF were added to a 250 mL round bottom flask containing *o*-toluic acid (5.00 g, 36.7 mmol) in 100 mL of dry DCM. The reaction mixture was heated to reflux temperature for 2 h. The solvent and excess $SOCl_2$ were then removed under reduced pressure to afford a yellow coloured liquid. The product was dissolved in 30 mL of dry DCM and then added dropwise to a 250 mL round bottom flask containing a stirring solution of distilled 2-amino-2-methyl-1-propanol (4.26 g, 47.7 mmol) and NEt_3 (7.68 mL, 55.1 mmol) in 100 mL of dry DCM at 0 °C. The reaction mixture was then stirred for 4 h at RT. The crude sample was washed once with 30 mL of 1 M solution of aqueous HCl and 2 × 30 mL of a saturated aqueous brine solution. The organic layer was then dried over anhydrous $MgSO_4$, filtered, and the solvent removed under reduced pressure to afford the *N*-(1-hydroxy-2-methylpropan-2-yl)-2-methylbenzamide intermediate as a white coloured powder in a 69.9% yield. The benzamide (5.32 g, 25.7 mmol) was dissolved in $SOCl_2$ (15.0 mL, 206 mmol) at 0 °C. The solution stirred at room temperature for 24 h, followed by addition of 100 mL of Et_2O. The precipitate was collected via vacuum filtration and dissolved in 50 mL of DCM. The solution was washed with a saturated aqueous solution of $NaHCO_3$ until the organic layer was neutral and then dried over anhydrous $MgSO_4$. After filtration, the solvent was removed under reduced pressure to yield **8** as a yellow coloured liquid. Yield: 4.07 g, 58.6%. NMR data (^{1}H, ^{13}C) matches reported literature data within experimental error [32].

^{1}H NMR (400.13 MHz, $CDCl_3$, δ): 7.86 (d, 1H, H6, $^{3}J_{1H–1H}$ = 7.78), 7.33–7.29 (m, 1H, H9), 7.21–7.17 (m, 2H, H7 & H8) 4.15 (s, 2H, H3), 2.53 (s, 3H, H11) 1.42 (s, 6H, H1) ppm. ^{13}C{^{1}H} NMR (100.61 MHz, $CDCl_3$, δ): 164.45 (C4), 138.92 (C10), 131.42 (C9), 131.27 (C8), 130.36 (C6), 125.93 (C5), 125.78 (C7), 79.52 (C3), 66.85 (C2), 28.06 (C1), 21.44 (C11) ppm.

*3.10. Synthesis of 4,4-Dimethyl-2-(2-((triphenylstannyl)methyl)phenyl)-4,5-dihydrooxazole (**4**)*

Compound **8** (0.50 g, 26.4 mmol) and 10 mL of dry Et_2O were added to a dry 50 mL Schlenk flask. The solution was cooled down to 0 °C and 1.6 M *n*-BuLi/hexane (1.82 mL, 2.91 mmol) was added dropwise to produce a dark red opaque solution and allowed to stir for 20 min. A solution of Ph_3SnCl (1.02 g, 26.4 mmol) in 15 mL of Et_2O was added dropwise to the lithiated mixture to produce a yellow coloured opaque solution and stirred for 1 h at 0 °C. The solvent was removed under reduced pressure and 10 mL of toluene was added. The mixture was filtered via gravity filtration and the solvent was removed under reduced pressure to yield a pale yellow coloured powder. The crude product was triturated with MeOH and the yellow supernatant removed. The residual solvent from the solid was removed under reduced pressure to yield white coloured crystals of **4**. ^{1}H and ^{13}C NMR experimental data are in good agreement with the reported literature [31]. Yield: 1.10 g, 77.4%. ^{1}H NMR (400.13, $CDCl_3$, δ): 7.77 (d, 1H, H9, $^{3}J_{1H–1H}$ = 7.8 Hz), 7.46–7.44 (m, 6H, H13), 7.36–7.31 (m, 9H, H14 & H15), 7.29–7.28 (m, 2H, H6 & H7), 7.12–7.10 (m, 1H, H8), 3.74 (s, 2H, H3), 3.57 (s, 2H, H11, $^{2}J_{1H–117/119Sn}$ = 75.5 Hz), 1.11 (s, 6H, H1) ppm. ^{13}C {^{1}H} NMR (100.61 MHz, $CDCl_3$, δ): 161.69 (C4), 143.53 (C10), 140.10 (C12), 136.97 (C14, $^{3}J_{13C–117/119Sn}$ = 34.7 Hz), 130.62 (C6), 129.91 (C9), 129.34 (C7), 128.55 (C15, $^{4}J_{13C–117/119Sn}$ = 11.0 Hz), 128.12 (C13, $^{2}J_{13C–117/119Sn}$ = 49.0 Hz), 124.37 (C5), 123.72 (C8), 77.58 (C3), 68.20 (C2), 28.24 (C1), 23.34 (C11) ppm. ^{119}Sn {^{1}H} NMR (149.21 MHz, $CDCl_3$, δ): −126.0 ppm. HRMS-DART (*m*/*z*): [M − C_6H_5] calculated for $^{12}C_{24}{}^{1}H_{24}{}^{14}N_1{}^{16}O_1{}^{120}Sn_1$: 462.08799; found 462.08871.

*3.11. Synthesis of 2-(2-((Dibromo(phenyl)stannyl)methyl)phenyl)-4,4-dimethyl-4,5-dihydrooxazole (**11**)*

A solution of **4** (2.46 g, 4.57 mmol) and 20 mL of DCM was added to a 100 mL Schlenk flask and cooled to 0 °C. A solution of Br_2 (0.466 mL, 9.14 mmol) in 10 mL of DCM was added dropwise and the reaction mixture stirred for 1 h at 0 °C. The solvent was removed under reduced pressure to yield a brown-yellow coloured powder. The crude product was triturated with MeOH and the yellow solution

was decanted off. The residual solvent was removed under reduced pressure to afford the product as a white coloured powder. Recrystallization of **11** (0.500 g) was achieved by dissolving the powder in a minimal amount of DCM (0.7 mL) and layering with hexanes (1.0 mL), followed by cooling to −20 °C overnight, yielding clear colourless crystals. Yield 2.05 g, 82.3%. ^{1}H NMR (400.13, $CDCl_3$, δ): 7.93 (d, 1H, H6, $^{3}J_{1H–1H}$ = 7.64 Hz), 7.54–7.52 (m, 2H, H8 & H9), 7.39–7.32 (m, 6H, H7, H13, H14 & H15), 4.05 (s, 2H, H3), 3.63 (s, 2H, H11, $^{2}J_{1H–117/119Sn}$ = 112.7 Hz), 1.25 (s, 6H, H1) ppm. ^{13}C {^{1}H} NMR (100.61 MHz, $CDCl_3$, δ): 166.48 (C4), 144.59(C12), 139.89 (C10), 133.91 (C14, $^{3}J_{13C–117/119Sn}$ = 60.0 Hz), 133.28 (C8), 130.54 (C9), 130.22 (C6), 130.18 (C7), 128.97 (C13, $^{2}J_{13C–117/119Sn}$ = 86.8 Hz), 126.80 (C15), 121.84(C5), 79.21 (C3), 69.27 (C2), 41.50 (C11), 27.67 (C1) ppm. ^{119}Sn {^{1}H} NMR (149.21 MHz, $CDCl_3$, δ): −248.2 ppm. HRMS-DART (*m*/*z*): [M + H] calculated for $^{12}C_{18}{}^{1}H_{20}{}^{79}Br_2{}^{14}N_1{}^{16}O_1{}^{120}Sn_1$: 543.89336; found 543.89537.

*3.12. Synthesis of 4,4-Dimethyl-2-(2-((phenylstannyl)methyl)phenyl)-4,5-dihydrooxazole (**13**)*

A suspension of **11** (0.50 g, 0.919 mmol) in 15 mL of dry EtOH was added dropwise to a solution of $NaBH_4$ (0.174 g, 4.70 mmol) in 5 mL of dry EtOH at 0 °C. The solution continued to stir at 0 °C for 1 h. Cold hexane (15 mL) was added to the solution and then quenched with 5 mL of chilled degassed distilled water. The mixture was extracted, and the organic layer was dried over anhydrous $MgSO_4$. The solution was filtered, and the solvent was removed under reduced pressure to yield the product as a colourless viscous oil. Yield = 0.305 g, 85.9%. ^{1}H NMR (400.13, C_6D_6, δ): 8.02 (d, 1H, H6, $^{2}J_{1H–1H}$ = 7.7 Hz), 7.51–7.49 (m, 2H, H14), 7.16–7.15 (m, 3H, H15 & H16), 7.03–7.01 (m, 2H, H7 & H8), 6.93–6.91 (m, 1H, H9), 5.94 (s, 2H, H12, $^{1}J_{117Sn–1H}$ = 1857 Hz, $^{1}J_{119Sn–1H}$ = 1943 Hz) 3.55 (s, 2H, H3), 3.07 (s, 2H, H11, $^{2}J_{117/119Sn–1H}$ = 76.1 Hz) ppm. ^{13}C {^{1}H} NMR (100.61 MHz, C_6D_6, δ): 161.64 (C4), 145.43 (C10), 140.53 (C13), 137.03 (C14), 130.72 (C8), 129.81 (C6), 129.31 (C7), 128.22 (C16), 128.13 (C15), 77.25 (C3), 68.23 (C2), 27.88 (C1), 21.86 (C11) ppm. ^{119}Sn {^{1}H} NMR (149.21 MHz, C_6D_6, δ): −221.02 ppm.

*3.13. Synthesis of Polymer (**15**)*

A solution of **13** (0.432 g, 1.119 mmol) in 3 mL of dry toluene was added dropwise to a dry Schlenk wrapped in Al foil containing Wilkinson's catalyst (0.0414 g, 0.045 mmol) in 10 mL of dry toluene at 0 °C. The solution continued to be stirred at 0 °C for 4 h and then the solvent was removed under reduced pressure. The crude product was dissolved in minimal dry THF (2 mL) and added dropwise to cold stirring hexanes (3 × 75 mL) and heptane (1 × 75 mL). The residual solvent was removed under reduced pressure to yield a pale-yellow powder of **15**. Yield = 0.096 g, 22.2%. ^{1}H NMR (400.13, C_6D_6, δ): 7.96–7.61 (m, 4H), 7.10–6.60 (m, 5H), 3.58–3.25 (m, 4H). Note: The methyl resonances were obscured by the presence of solvent and not assigned. ^{119}Sn {^{1}H} NMR (149.21 MHz, C_6D_6, δ): −183.8 ppm.

4. Conclusions

Sets of both oxazolines containing triphenyl stannanes, dibromidooxazoline stannanes, and stannane dihydrides were prepared and characterized. A monochloridooxazoline stannane was also prepared. Crystallographic studies of five different κ^2-*C,N* tin-oxazoline compounds adopt a preferentially distorted trigonal bipyramidal geometry around Sn, even in the absence of a strong-withdrawing ligand *trans* to the Sn–N bond. Short Sn–N bonds were observed for the halo containing tin oxazolines. The oxazoline organotin monomers form an interesting class of compounds for investigating Sn hypercoordination by DFT modelling, particularly as they have two potentially coordinating atoms (N,O). We are currently extending these studies to consider the relative energy differences between oxazoline coordination isomers, the impact of solvation, and the feasibility of predicting ^{119}Sn chemical shifts in these systems by NMR calculations. Evidence for Sn oxazoline polymers prepared by transition metal catalyzed dehydrocoupling of their respective dihydrides was demonstrated; however, purification and isolation proved difficult. The difficulty in preparing high molecular weight examples stems in part from the extreme sensitivity of the dihydride

monomers, which begin to decompose prior to polymerization. Efforts to identify more flexible, yet stable oxazoline tin derivatives is now underway.

Supplementary Materials: The following are available online at http://www.mdpi.com/2304-6740/8/5/35/s1, NMR spectra (^{1}H, ^{13}C, ^{119}Sn, and 2D NMR) in Figures S1–S57 and computational data in Tables S1–S42. Crystallographic data for compounds **4** (CCDC# 1987221), **7** (CCDC# 1987224), **9** (CCDC# 1987220), **10** (CCDC# 1987222), and **11** (CCDC# 1987223) were deposited with the Cambridge Crystallographic Data Base. The CIF and checkCIF output files are included.

Author Contributions: D.N.B. carried out the research work; D.A.F. and R.A.G. lead the research project and drafted the manuscript; A.J.L. was the crystallographer for all the structures in this manuscript; R.S.W. carried out all the computational calculations. All authors have read and agreed to the published version of the manuscript.

Funding: This work was supported by the NSERC Discovery Grant program.

Acknowledgments: The computational studies for R. Stephen Wylie were made possible by the facilities of Compute/Calcul Canada and the Ryerson Analytical Facility.

Conflicts of Interest: The authors declare no conflict of interest.

References

1. Caseri, W. Polystannanes: Processible molecular metals with defined chemical structures. *Chem. Soc. Rev.* **2016**, *45*, 5187–5199. [CrossRef] [PubMed]
2. Deacon, P.R.; Devylder, N.; Hill, M.S.; Mahon, M.F.; Molloy, K.C.; Price, G.J. Organotin compounds bearing mesogenic sidechains: Synthesis, X-ray structures and polymerisation chemistry. *J. Organomet. Chem.* **2003**, *687*, 46–56. [CrossRef]
3. Lu, V.Y.; Tilley, T.D. Poly(diaryl)stannanes: Influence of substituents on the σ–σ* transition energy. *Macromolecules* **2000**, *33*, 2403–2412. [CrossRef]
4. Harrypersad, S.; Foucher, D. Alternating polystannanes: Syntheses and properties. *Chem. Commun.* **2015**, *51*, 7120–7123. [CrossRef]
5. Choffat, F.; Buchmüller, Y.; Mensing, C.; Smith, P.; Caseri, W. Poly(di(ω-alkylphenyl)stannane)s. *J. Inorg. Organomet. Polym. Mater.* **2009**, *19*, 166–175. [CrossRef]
6. Imori, T.; Lu, V.; Cai, H.; Tilley, T.D. Metal-Catalyzed Dehydropolymerization of Secondary Stannanes to High Molecular Weight Polystannanes. *J. Am. Chem. Soc.* **1995**, *117*, 9931–9940. [CrossRef]
7. Pau, J.; Lough, A.J.; Wylie, R.S.; Gossage, R.A.; Foucher, D.A. Proof of Concept Studies Directed Towards Designed Molecular Wires: Property Driven Synthesis of Air and Moisture-Stable Polystannanes. *Chem. A Eur. J.* **2017**, *57*, 14367–14374. [CrossRef]
8. Pau, J.; D'Amaral, G.M.; Lough, A.J.; Wylie, R.S.; Foucher, D.A. Synthesis and Characterization of Readily Modified Poly(aryl)(alkoxy)stannanes by use of Hypercoordinated Sn Monomers. *Chem. A Eur. J.* **2018**, *24*, 18762–18771. [CrossRef]
9. Khan, A.; Foucher, D.A. Hypercoordinate compounds of the group 14 elements containing κ2-C,N-, C,O-, C,S- and C,P-ligands. *Coord. Chem. Rev.* **2016**, *312*, 41–66. [CrossRef]
10. Musher, J.I. The Chemistry of Hypervalent Molecules. *Angew. Chem. Int. Ed. Engl.* **1969**, *8*, 54–68. [CrossRef]
11. Minyaev, R.M.; Gribanova, T.N.; Minkin, V.I. *Comprehensive Inorganic Chemistry II*, 2nd ed.; Reedijk, J., Poeppelmeier, K., Eds.; Elsevier, Ltd.: Oxford, UK, 2013; Volume 9, pp. 109–132.
12. Nandi, A.; Kozuch, S. History and Future of Dative Bonds. *Chem. A Eur. J.* **2020**, *26*, 759–772. [CrossRef] [PubMed]
13. Van Koten, G.; Noltes, J.G.; Spek, A.L. Crystal and Molecular Structure of C,N-{2-[(dimethylamino)phenyl} diphenyltin bromide J. *Organomet. Chem.* **1976**, *118*, 183–189. [CrossRef]
14. Boyer, J.; Breliere, C.; Corriu, R.J.P.; Kpoton, A.; Poirier, M.; Royo, G. Enhancement of Si–H bond reactivity in pentacooridinated structures. *J. Organomet. Chem.* **1986**, *311*, C39–C43. [CrossRef]
15. Breliere, C.; Carre, F.; Corriu, R.J.P.; De Saxce, A.; Poirier, M.; Royo, G. Pentacoordinate silicon and germanium derivatives: Molecular structure. *J. Organomet. Chem.* **1981**, *205*, C1–C3. [CrossRef]
16. De Wit, P.P.; Van Der Kooi, H.O.; Wolters, J. An Intriguing plumbylene: Bis[2-(dimethylaminomethyl)-phenyl]lead. *J. Organomet. Chem.* **1981**, *216*, 9–11. [CrossRef]

17. Khan, A.; Pau, J.; Loungxay, J.; Magobenny, T.; Wylie, R.S.; Lough, A.J.; Foucher, D. Hypercoordinated organotin(IV) compounds containing C,O- and C,N- chelating ligands: Synthesis, characterisation, DFT studies and polymerization behavior. *J. Organomet. Chem.* **2019**, *900*, 120910. [CrossRef]
18. Meyers, A.I.; Mihelich, E.D. The Synthetic Utility of 2-Oxazolines. *Angew. Chem. Int. Ed.* **1976**, *15*, 270–281. [CrossRef]
19. Gomez, M.; Muller, G.; Rocamora, M. Coordination chemistry of oxazoline ligands. *Coord. Chem. Rev.* **1999**, *193–195*, 769–835. [CrossRef]
20. Adjei, J.A.; Lough, A.J.; Gossage, R.A. Synthesis and characterisation of C,N κ2-N,O oxazoline-enolate complexes of nickel(II): Explorations in coordination chemistry and metal mediated polymerization. *RSC Adv.* **2019**, *9*, 3956–3964. [CrossRef]
21. Adams, N.; Schubert, U.S. Poly(2-oxazolines) in biological and biomedical application contexts Adv. *Drug Deliv. Rev.* **2007**, *59*, 1504–1520. [CrossRef]
22. Krolikiewicz, H.; Vorbrüggen, K. A simple synthesis of Δ2-oxazolines, Δ2-oxazines, Δ2-thiazolines and 2-substituted benzoxazoles. *Tetrahedron* **1993**, *49*, 9353–9372. [CrossRef]
23. Lee, J.D.; Kim, H.S.; Han, W.S.; Kang, S.O. Chiral organotin complexes stabilized by C,N-chelating oxazolinyl-o-carboranes. *J. Organomet. Chem.* **2010**, *695*, 463–468. [CrossRef]
24. Selvaratnam, S.; Mun, K.; Das, V.G.K. Synthesis and structural characterization of (2-oxazolinylthienyl) tetraorganotin (IV) compounds. *J. Organomet. Chem.* **1994**, *464*, 143–148. [CrossRef]
25. Stol, M.; Snelders, D.J.M.; De Pater, J.J.M.; Van Klink, G.P.M.; Kooijman, H.; Spek, A.L.; Van Koten, G. Synthesis and structural characterization of lithium and trimethyltin complexes of 2,6-bis(oxazolinyl)phenyl. *Organometallics* **2005**, *24*, 743–749. [CrossRef]
26. Jastrzebski, J.T.B.H.; Wehman, E.; Boersma, J.; van Koten, G. Synthesis and structure of [2-(4,4-dimethyl-2-oxazoline)-5-methylphenyl]methylphenyltin bromide. A novel triorganotin halide having a configurationally stable chiral tin center. *J. Organomet. Chem.* **1991**, *409*, 157–162. [CrossRef]
27. Cmoch, P.; Urbańczyk-Lipkowska, Z.; Petrosyan, A.; Stępień, A.; Staliński, K. The 1H, 13C, 15N and117Sn NMR study of the intramolecular Sn–N interaction in tri- and tetraorganotin compounds containing the chiral 2-(4-isopropyl-2-oxazolinyl)-5-phenyl ligand. *J. Mol. Struct.* **2005**, *733*, 29–39. [CrossRef]
28. Staliński, K.; Urbańczyk-Lipkowska, Z.; Cmoch, P.; Rupnicki, L.; Grachev, A. New chiral tin compounds containing the 2-(4-isopropyl-2-oxazolinyl)-5-phenyl ligand. *J. Organomet. Chem.* **2006**, *691*, 2394–2402. [CrossRef]
29. Rupnicki, L.; Urbańczyk-Lipkowska, Z.; Stępień, A.; Cmoch, P.; Pianowski, Z.; Staliński, K. New distannanes containing the chiral 2-(4-isopropyl-2-oxazolinyl)-5-phenyl ligand. *J. Organomet. Chem.* **2005**, *690*, 3690–3696. [CrossRef]
30. Matkowska, D.; Gola, M.; Śniezek, M.; Cmoch, P.; Staliński, K. Structural assignment of organotin hydrides containing the oxazoline ligand. *J. Organomet. Chem.* **2007**, *692*, 2036–2045. [CrossRef]
31. Bonnardel, P.-A.; Parish, R.V. Organomercury(II) and organotin(IV) compounds with nitrogen-containing substituents. *J. Organomet. Chem* **1996**, *515*, 221–232. [CrossRef]
32. Gschwend, H.W.; Hamdan, A. Ortho-Lithiation of Aryloxazolines. *J. Org. Chem.* **1975**, *40*, 2008–2009. [CrossRef]
33. Addison, A.W.; Rao, T.N.; Reedijk, J.; van Rijn, J.; Verschoor, G.C. Synthesis, Structure, and Spectroscopic Properties of Copper(II) Compounds containing Nitrogen–Sulphur Donor Ligands; the Crystal and Molecular Structure of Aqua[l,7-bis(N-methylbenzimidazol-2′-yl)-2,6-dithiaheptane]copper(II) Perchlorate. *J. Chem. Soc. Dalton. Trans.* **1984**, 1349–1356. [CrossRef]
34. Jurkschat, K.; Tzschach, A.; Meunier-Piret, J. Crystal and Molecular Structure of 1-Aza-5-stannan-5-methyltricyclo[3,3,3]undecane. Evidence for a transannular donor–acceptor interaction in a tetraorganotin compound. *J. Organomet. Chem.* **1986**, *315*, 45–49. [CrossRef]
35. Baukov, Y.I.; Tandura, S.N.; Rappoport, Z. *The Chemistry of Organic Germanium, Tin and Lead Compounds*; John Wiley & Sons, Ltd.: New York, NY, USA, 2002. [CrossRef]
36. Munguia, T.; Lo, M.; Cervantes-Lee, F.; Pannell, K.H. Intramolecular Chalcogen−Tin Interactions in (o-MeE-C6H4)CH2SnPh3−nCln (E = S, O; n = 0, 1, 2), Characterized by X-ray Diffraction and 119Sn Solution and Solid-State NMR. *Inorg. Chem.* **2007**, *46*, 1305–1314. [CrossRef]
37. Novák, P.; Padělková, Z.; Císařová, I.; Kolářová, L.; Růžička, A.; Holeček, J. Structural study of C,N-chelated monoorganotin(IV) halides. *Appl. Organomet. Chem.* **2006**, *20*, 226–232. [CrossRef]

38. Švec, P.; Růžičková, Z.; Vlasák, P.; Turek, J.F.; De Proft, F.; Růžička, A. Expanding the family of C,N-chelated organotin(IV) pseudohalides: Synthesis and structural Characterization. *J. Organomet. Chem.* **2016**, *801*, 14–23. [CrossRef]
39. Whittleton, S.R.; Boyd, R.J.; Grindley, T.B. Evaluation of effective core potentials and basis sets for the prediction of the geometries of alkyltin halides. *J. Phys. Chem. A* **2006**, *110*, 5893–5896. [CrossRef]
40. Matczak, P. Assessment of B3LYP combined with various ECP basis sets for systems containing Pd, Sn, and Pb. *Comput. Theor. Chem.* **2012**, *983*, 25–30. [CrossRef]
41. Perdew, J.P. Unified theory of exchange and correlation beyond the local density approximation. In *Electronic Structure of Solids' 91*; Ziesche, P., Eschig, H., Eds.; Akademie Verlag: Berlin, Germany, 1991; pp. 11–20.
42. Perdew, J.P.; Burke, K.; Ernzerhof, M. Generalized gradient approximation made simple. *Phys. Rev. Lett.* **1996**, *77*, 3865–3868. [CrossRef]
43. Grimme, S.; Ehrlich, S.; Goerigk, L. Effect of the damping function in dispersion corrected density functional theory. *J. Comput. Chem.* **2011**, *32*, 1456–1465. [CrossRef]
44. Goerigk, L.; Mehta, N. A Trip to the Density Functional Theory Zoo: Warnings and Recommendations for the User. *Aust. J. Chem.* **2019**, *72*, 563–573. [CrossRef]
45. Zhao, Y.; Schultz, N.E.; Truhlar, D.G. Design of Density Functionals by Combining the Method of Constraint Satisfaction with Parametrization for Thermochemistry, Thermochemical Kinetics, and Noncovalent Interactions. *J. Chem. Theory Comput.* **2006**, *2*, 364–382. [CrossRef] [PubMed]
46. Goerigk, L.; Grimme, S. A thorough benchmark of density functional methods for general main group thermochemistry, kinetics, and noncovalent interactions. *Phys. Chem. Chem. Phys.* **2011**, *13*, 6670–6688. [CrossRef] [PubMed]
47. Choffat, F.; Smith, P.; Caseri, W. Polystannanes: Polymers of a Molecular, Jacketed Metal-Wire Structure. *Adv. Mater.* **2008**, *20*, 2225–2229. [CrossRef]
48. Khan, A.; Patel, A.; Komejan, S.; Lombardi, C.; Lough, A.J.; Foucher, D.A. Reduction of C,O-chelated organotin(IV) dichlorides and dihydrides leading to protected polystannanes. *J. Organomet. Chem.* **2015**, *776*, 180–191. [CrossRef]
49. Sheldrick, G.M. SHELXT—Integrated space-group and crystal-structure determination. *Acta Cryst.* **2015**, *C71*, 3–8. [CrossRef]
50. Frisch, M.J.; Trucks, G.W.; Schlegel, H.B.; Scuseria, G.E.; Robb, M.A.; Cheeseman, J.R.; Scalmani, G.; Barone, V.; Mennucci, B.; Petersson, G.A.; et al. *Gaussian 16, Revision C.01*; Gaussian. Inc.: Wallingford, CT, USA, 2019.
51. Pritchard, B.P.; Altarawy, D.; Didier, B.; Gibson, T.D.; Windus, T.L. A New Basis Set Exchange: An Open, Up-to-date Resource for the Molecular Sciences Community. *J. Chem. Inf. Model.* **2019**, *59*, 4814–4820. [CrossRef]
52. O'Boyle, N.M.; Banck, M.; James, C.A.; Morley, C.; Vandermeersch, T.; Hutchison, G.R. Open Babel: An open chemical toolbox. *J. Cheminform.* **2011**, *3*, 33. [CrossRef]
53. Schöler, S.; Wahl, M.H.; Wurster, N.I.C.; Puls, A.; Hättig, C.; Dyker, G. Bidentate cycloimidate palladium complexes with aliphatic and aromatic anagostic bonds. *Chem. Commun.* **2014**, *50*, 5909–5911. [CrossRef]
54. Sedelmeier, J.; Hammerer, T.; Bolm, C. C1-Symmetric Oxazolinyl Sulfoximines as Ligands in Copper-Catalyzed Asymmetric Mukaiyama Aldol Reactions. *Org. Lett.* **2008**, *10*, 917–920. [CrossRef]